

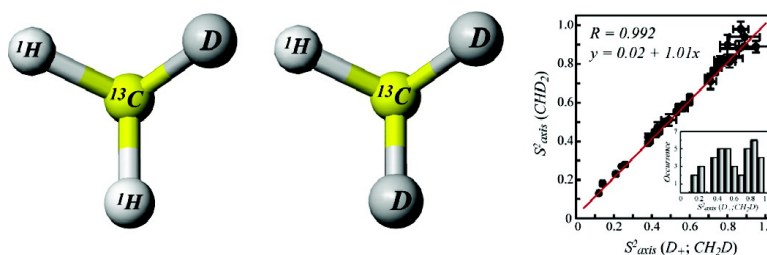
Article

# Probing Side-Chain Dynamics in High Molecular Weight Proteins by Deuterium NMR Spin Relaxation: An Application to an 82-kDa Enzyme

Vitali Tugarinov, Jason E. Ollerenshaw, and Lewis E. Kay

*J. Am. Chem. Soc.*, **2005**, 127 (22), 8214-8225 • DOI: 10.1021/ja0508830 • Publication Date (Web): 13 May 2005

Downloaded from <http://pubs.acs.org> on March 25, 2009



## More About This Article

Additional resources and features associated with this article are available within the HTML version:

- Supporting Information
- Links to the 8 articles that cite this article, as of the time of this article download
- Access to high resolution figures
- Links to articles and content related to this article
- Copyright permission to reproduce figures and/or text from this article

[View the Full Text HTML](#)

## Probing Side-Chain Dynamics in High Molecular Weight Proteins by Deuterium NMR Spin Relaxation: An Application to an 82-kDa Enzyme

Vitali Tugarinov, Jason E. Ollerenshaw, and Lewis E. Kay\*

Contribution from the Protein Engineering Network Centers of Excellence and Departments of Medical Genetics, Biochemistry, and Chemistry, The University of Toronto, Toronto, Ontario M5S 1A8, Canada

Received February 10, 2005; E-mail: kay@pound.med.utoronto.ca

**Abstract:** New NMR experiments for the measurement of side-chain dynamics in high molecular weight (~100 kDa) proteins are presented. The experiments quantify  $^2\text{H}$  spin relaxation rates in  $^{13}\text{CH}_2\text{D}$  or  $^{13}\text{CHD}_2$  methyl isotopomers and, for applications to large systems, offer significant gains both in sensitivity (2–3-fold) and resolution over previously published HSQC schemes. The methodology has been applied to investigate Ile dynamics in the 723-residue, single polypeptide chain enzyme, malate synthase G. Methyl-axis order parameters,  $S_{\text{axis}}$ , characterizing the amplitudes of motion of the methyl groups, have been derived from both  $^{13}\text{CH}_2\text{D}$  and  $^{13}\text{CHD}_2$  probes and are in excellent agreement. The distribution of order parameters is trimodal, reflecting the range of dynamics that are available to Ile residues. A reasonable correlation is noted between  $S_{\text{axis}}^2$  and inverse temperature factors from X-ray studies of the enzyme. The proposed methodology significantly extends the range of protein systems for which side-chain dynamics can be studied.

### Introduction

Protein molecules are inherently dynamic, and it is becoming increasingly apparent that often these dynamics are critical for function.<sup>1–5</sup> As a result, efforts in developing both experimental and theoretical tools for studying motional processes in a variety of different systems have intensified in the past several years. NMR spectroscopy is a particularly powerful experimental probe of molecular dynamics because a wide range of motional time scales can be studied and because site-specific information is available.<sup>6–11</sup> NMR studies of protein backbone dynamics<sup>6,12</sup> are essentially routine now, and investigations of side-chain dynamics, largely involving  $^2\text{H}$  spin relaxation measurements,<sup>13–16</sup> are also increasing in number. Applications to date have focused primarily on small proteins, less than approximately 30 kDa,

since until recently NMR approaches for the study of larger systems have been limited both by sensitivity and resolution. However, many important biomolecules are in excess of 30 kDa, and the need for more sensitive experiments that can access larger systems is thus apparent.

Here we describe a suite of new  $^2\text{H}$ -based spin relaxation experiments to study the dynamics of methyl-containing side chains in proteins on the order of 100 kDa in molecular weight, significantly increasing the range of biomolecular systems that can be investigated. An application to a 723-residue enzyme, malate synthase G<sup>17,18</sup> (MSG), is presented, focusing on Ile- $\delta 1$  positions in the protein. Issues of sensitivity and resolution are particularly important in such applications, and we present new labeling schemes and pulse sequences that are optimal in this regard. As with the development of any new experiment, it is important to validate the methodology. We show that very similar order parameters, characterizing the amplitudes of side-chain dynamics, are obtained both from experiments that make use of different coherences to quantify dynamics from within a given methyl probe ( $^{13}\text{CH}_2\text{D}$ ) and from schemes that monitor dynamics with different methyl probes ( $^{13}\text{CH}_2\text{D}$  and  $^{13}\text{CHD}_2$ ). A “three-pronged” distribution of Ile  $\delta 1$  order parameters is obtained that is very similar to that noted in molecular dynamics simulations,<sup>19</sup> reflecting the different classes of  $\chi_1$ ,  $\chi_2$  fluctuations that are accessible to such side chains. Finally, a reasonable

- (1) Karplus, M.; McCammon, J. A. *Annu. Rev. Biochem.* **1983**, *53*, 263–300.
- (2) Frauenfelder, H.; Sligar, S. G.; Wolynes, P. G. *Science* **1991**, *254*, 1598–1603.
- (3) Fersht, A. *Structure and Mechanism in Protein Science*, 2nd ed.; W. H. Freeman: New York, 1999.
- (4) Dobson, C. M.; Karplus, M. *Curr. Opin. Struct. Biol.* **1999**, *9*, 92–101.
- (5) Kern, D.; Zuiderweg, E. R. *Curr. Opin. Struct. Biol.* **2003**, *13*, 748–757.
- (6) Peng, J. W.; Wagner, G. *Methods Enzymol.* **1994**, *239*, 563–596.
- (7) Kay, L. E. *Nat. Struct. Biol. NMR Suppl.* **1998**, *5*, 513–516.
- (8) Ishima, R.; Torchia, D. A. *Nat. Struct. Biol.* **2000**, *7*, 740–743.
- (9) Palmer, A. G.; Kroenke, C. D.; Loria, J. P. *Methods Enzymol.* **2001**, *339*, 204–238.
- (10) Korzhnev, D. M.; Billeter, M.; Arseniev, A. S.; Orekhov, V. Y. *Prog. Nucl. Magn. Reson. Spectrosc.* **2001**, *38*, 197–266.
- (11) Fushman, D.; Cowburn, D. *Methods Enzymol.* **2001**, *339*, 109–126.
- (12) Kay, L. E.; Torchia, D. A.; Bax, A. *Biochemistry* **1989**, *28*, 8972–8979.
- (13) Muhandiram, D. R.; Yamazaki, T.; Sykes, B. D.; Kay, L. E. *J. Am. Chem. Soc.* **1995**, *117*, 11536–11544.
- (14) Yang, D.; Mittermaier, A.; Mok, Y.; Kay, L. E. *J. Mol. Biol.* **1998**, *276*, 939–954.
- (15) Millet, O.; Muhandiram, D. R.; Skrynnikov, N. R.; Kay, L. E. *J. Am. Chem. Soc.* **2002**, *124*, 6439–6448.
- (16) Skrynnikov, N. R.; Millet, O.; Kay, L. E. *J. Am. Chem. Soc.* **2002**, *124*, 6449–6460.

- (17) Molina, I.; Pellicer, M. T.; Badia, J.; Aguilar, J.; Baldoma, L. *Eur. J. Biochem.* **1994**, *224*, 541–548.
- (18) Howard, B. R.; Endrizzi, J. A.; Remington, S. J. *Biochemistry* **2000**, *39*, 3156–3168.
- (19) Best, R. B.; Clarke, J.; Karplus, M. *J. Am. Chem. Soc.* **2004**, *126*, 7734–7735.

correlation between order parameters and inverse temperature factors from X-ray studies of the enzyme is noted.

## Materials and Methods

**NMR Samples.** A pair of MSG samples labeled with different Ile- $\delta 1$  methyl isotopomers was used in the present study: (i) U- $^{15}\text{N}, ^2\text{H}$  Ile $\delta 1$ - $^{13}\text{CH}_2\text{D}$ -MSG and (ii) U- $^{15}\text{N}, ^2\text{H}$  Ile $\delta 1$ - $^{13}\text{CHD}_2$ -MSG. Both samples were prepared as described in detail previously<sup>20,21</sup> with U- $^2\text{H}$ -D-glucose (CIL, Andover, MA) as the main carbon source,  $^{15}\text{NH}_4\text{Cl}$  (CIL, Andover, MA) as the nitrogen source, and with the addition of 100 mg of 4- $^{13}\text{C}$ -4- $^2\text{H}$ -3,3- $^2\text{H}$ - $\alpha$ -ketobutyrate (Ile  $\delta 1$ - $^{13}\text{CH}_2\text{D}$ -labeling) or 4- $^{13}\text{C}$ -4,4- $^2\text{H}$ -3,3- $^2\text{H}$ - $\alpha$ -ketobutyrate (Ile  $\delta 1$ - $^{13}\text{CHD}_2$ -labeling) to the growth media 1 h. prior to induction. All sodium salts of the  $\alpha$ -ketobutyric acids used as biosynthetic precursors in this work were obtained in protonated form at position 3 from Isotec (Miamisburg, OH) and used without further purification. The 3,3- $^1\text{H}$  positions have been exchanged to  $^2\text{H}$  following the procedure of Gardner and Kay.<sup>22</sup> The U- $^{15}\text{N}, ^2\text{H}$  Ile $\delta 1$ - $^{13}\text{CH}_2\text{D}$ -labeled sample of MSG was found to contain approximately 10% of the  $^{13}\text{CHD}_2$  isotopomer due to a 10%  $^{13}\text{CHD}_2$  isotopomer impurity in the precursor (i.e., 10% sodium salt of 4- $^{13}\text{C}$ -4,4- $^2\text{H}$ -3,3- $^2\text{H}$ - $\alpha$ -ketobutyric acid). The concentration of protein in both NMR samples was adjusted to  $0.80 \pm 0.05$  mM; samples contained 99.9%  $\text{D}_2\text{O}$ , 25 mM sodium phosphate, pH 7.1 (uncorrected), 20 mM  $\text{MgCl}_2$ , 0.05%  $\text{NaN}_3$ , and 5 mM DTT. A third sample, U- $^{15}\text{N}, ^2\text{H}$  Ile $\delta 1$ - $^{13}\text{CH}_3$  Leu, Val- $^{13}\text{CH}_3, ^{12}\text{CD}_3$ -labeled MSG, prepared as described earlier<sup>21,23</sup> and dissolved in 92%  $\text{H}_2\text{O}/8\%$   $\text{D}_2\text{O}$  ( $\sim 0.5$  mM in protein), was used for  $^{15}\text{N}$  relaxation and translational diffusion measurements to establish the rotational correlation time of MSG in  $\text{D}_2\text{O}$  (see later discussion).

**Deuterium Relaxation Measurements.** All  $^2\text{H}$  and  $^{15}\text{N}$  spin relaxation experiments were performed on a 600 MHz Varian Inova spectrometer (37 °C) equipped with a cryogenically cooled probe. NMR data sets recorded with the pulse scheme of Figure 2 (U- $^{15}\text{N}, ^2\text{H}$  Ile $\delta 1$ - $^{13}\text{CH}_2\text{D}$ -MSG) comprised [120, 576] complex points in the  $^{13}\text{C}, ^1\text{H}$  dimensions with corresponding acquisition times of [79 ms, 64 ms]. A relaxation delay of 1.5 s was used along with 16 scans/FID. A pair of FIDs was recorded for each complex  $t_1$  point corresponding to  $\phi 5 = \phi 6 = -x$  and  $\phi 5 = \phi 6 = x$  so that singlet components were obtained for each correlation (see later discussion). Thus, the net acquisition time for each experiment is  $\sim 3.3$  h.  $R^Q(D_+)$ ,  $R^Q(D_z)$ ,  $R^Q(D_+D_z + D_zD_+)$ ,  $R^Q(3D_z^2 - 2)$  relaxation rates were recorded with parametrically varied delays  $T$  (A–D in Figure 2) of (0.05, 0.18, 0.38, 0.59, 0.82, 1.08, 1.36, 1.70) ms, (0.1, 7.0, 15.0, 23.5, 32.9, 43.1, 54.5, 70.0) ms, (0.05, 0.21, 0.44, 0.69, 0.96, 1.30, 1.70) ms, and (0.1, 10.0, 21.0, 32.0, 45.0, 59.0, 80.0) ms, respectively. NMR data sets recorded with the sequence of Figure 6 (U- $^{15}\text{N}, ^2\text{H}$  Ile $\delta 1$ - $^{13}\text{CHD}_2$ -MSG) consisted of [84, 576] complex points in the  $^{13}\text{C}, ^1\text{H}$  dimensions, corresponding to acquisition times of [55 ms, 64 ms]. A relaxation delay of 2.0 s was used (to partially account for the significantly longer  $^1\text{H}$   $T_1$  values in the  $^{13}\text{CHD}_2$ -labeled sample) along with 24 scans/FID, for net recording times of  $\sim 140$  min/experiment. Transverse relaxation rates in the  $^{13}\text{CHD}_2$ -labeled sample were recorded with delays  $T$  of (0.05, 0.18, 0.38, 0.59, 0.82, 1.08, 1.36, 1.70) ms. All NMR spectra were processed using the NMRPipe/NMRDraw suite of programs and associated software.<sup>24</sup> Rates were obtained by fitting peak intensities to a monoexponential decay function,  $A\exp(-RT)$ , where  $R$  is the relaxation rate and  $T$  is the relaxation delay. Errors were estimated by a Monte Carlo analysis.<sup>25</sup> Average errors of 3.9, 5.3, 4.5, and 8.6% were obtained

for the  $R^Q(D_+)$ ,  $R^Q(D_z)$ ,  $R^Q(D_+D_z + D_zD_+)$ ,  $R^Q(3D_z^2 - 2)$  rates, respectively, for U- $^{15}\text{N}, ^2\text{H}$  Ile $\delta 1$ - $^{13}\text{CH}_2\text{D}$ -MSG and 2.8% for the  $^2\text{H}$  transverse rates in U- $^{15}\text{N}, ^2\text{H}$  Ile $\delta 1$ - $^{13}\text{CHD}_2$ -MSG.

As described in the legend to Figure 2, a field of 2 kHz was used for  $^2\text{H}$  pulses, corresponding to a  $180^\circ$  pulse width of 250  $\mu\text{s}$ . This pulse width is approximately 10% of the average  $^2\text{H}$  transverse relaxation time (2.2 ms) and substantially longer than the shortest relaxation delay (50  $\mu\text{s}$ ) used in  $T_2$  relaxation experiments. Simulations establish that there are no errors in the measured relaxation times from the finite pulse length, so long as the phase of the  $^2\text{H}$  refocusing pulse is cycled over the four quadrature phases ( $x, y, -x, -y$ ) so that the “effective” trajectory of the magnetization during the refocusing pulse (averaged over the four pulse phases) becomes independent of the relaxation delay. Errors are surprisingly small ( $<5\%$  for  $^2\text{H}$  offsets  $\leq 1$  ppm at 600 MHz  $^1\text{H}$  frequency) even if  $^2\text{H}$   $180^\circ_x$  pulses exclusively are employed for refocusing.

Millet et al. have developed experiments for the measurement of five deuterium relaxation rates in  $^{13}\text{CH}_2\text{D}$  methyl groups of small proteins.<sup>15</sup> These rates quantify the relaxation of  $D_+$ ,  $D_z$ ,  $D_+D_z + D_zD_+$ ,  $3D_z^2 - 2$ , and  $D_+^2$  elements (the first two and last three operators are referred to as “rank 1” and “rank 2” in the text). The relaxation rates of the five elements are given by:<sup>26</sup>

$$R^Q(D_+) = (1/80)(2\pi e^2 q Q/h)^2 [9J(0) + 15J(\omega_D) + 6J(2\omega_D)] \quad (1a)$$

$$R^Q(D_z) = (3/40)(2\pi e^2 q Q/h)^2 [J(\omega_D) + 4J(2\omega_D)] \quad (1b)$$

$$R^Q(D_+D_z + D_zD_+) = (1/80)(2\pi e^2 q Q/h)^2 [9J(0) + 3J(\omega_D) + 6J(2\omega_D)] \quad (1c)$$

$$R^Q(3D_z^2 - 2) = (3/40)(2\pi e^2 q Q/h)^2 [3J(\omega_D)] \quad (1d)$$

$$R^Q(D_+^2) = (3/40)(2\pi e^2 q Q/h)^2 [J(\omega_D) + 2J(2\omega_D)] \quad (1e)$$

where  $(e^2 q Q/h)$  is a quadrupolar coupling constant (167 kHz<sup>27</sup> used in this work). Here the following function was used for  $J(\omega)$ :<sup>28,29</sup>

$$J(\omega) = a^2 S_{\text{axis}}^2 \left[ \frac{A_1 \tau_1}{1 + (\omega \tau_1)^2} + \frac{A_2 \tau_2}{1 + (\omega \tau_2)^2} + \frac{A_3 \tau_3}{1 + (\omega \tau_3)^2} \right] + (1 - a^2 S_{\text{axis}}^2) \frac{\tau'}{1 + (\omega \tau')^2} \quad (2)$$

where  $S_{\text{axis}}$  is the generalized order parameter of the methyl threefold symmetry axis (located along the  $\text{C}^{\gamma 1}-\text{C}^{\delta 1}$  bond in Ile),  $a = (3 \cos^2(\theta) - 1)/2$ ,  $\theta$  is the angle between the C–D bond and the methyl threefold symmetry axis ( $a^2 = 1/9$  was used throughout this work),  $A_1 = (3/4) \sin^4(\alpha)$ ,  $A_2 = 3 \sin^2(\alpha) \cos^2(\alpha)$ ,  $A_3 = [(3/2) \cos^2(\alpha) - 0.5]^2$ ,  $\tau_1 = (4D_{\parallel} + 2D_{\perp})^{-1}$ ,  $\tau_2 = (D_{\parallel} + 5D_{\perp})^{-1}$ ,  $\tau_3 = (6D_{\perp})^{-1}$ ,  $D_{\parallel}$  and  $D_{\perp}$  are the principal components of the tensorial diffusion tensor,  $\alpha$  is the angle between the  $\text{C}^{\gamma 1}-\text{C}^{\delta 1}$  bond vector and the unique diffusion axis, and  $1/\tau' = 1/\tau_f + 1/\tau_{\text{c,eff}}$  with  $\tau_{\text{c,eff}} = (2D_{\parallel} + 4D_{\perp})^{-1}$  is the effective correlation time of overall rotation. Direction cosines for the  $\text{C}^{\gamma 1}-\text{C}^{\delta 1}$  vectors of Ile residues were obtained from the X-ray coordinates of MSG<sup>18</sup> (PDB ID 1d8c).

**Determination of the Rotational Diffusion Tensor of MSG.** An accurate global rotational diffusion tensor, usually obtained from  $^{15}\text{N}$  relaxation data of backbone amides, is required for the interpretation of  $^2\text{H}$  relaxation rates in terms of dynamic parameters (especially generalized order parameters of the methyl symmetry axis,  $S_{\text{axis}}$ ). The samples used in this study for  $^2\text{H}$  relaxation measurements were in

(20) Tugarinov, V.; Hwang, P. M.; Ollerenshaw, J. E.; Kay, L. E. *J. Am. Chem. Soc.* **2003**, *125*, 10420–10428.

(21) Tugarinov, V.; Kay, L. E. *J. Biomol. NMR* **2004**, *28*, 165–172.

(22) Gardner, K. H.; Kay, L. E. *J. Am. Chem. Soc.* **1997**, *119*, 7599–7600.

(23) Tugarinov, V.; Choy, W. Y.; Orekhov, V. Y.; Kay, L. E. *Proc. Natl. Acad. Sci. U.S.A.* **2005**, *102*, 622–627.

(24) Delaglio, F.; Grzesiek, S.; Vuister, G. W.; Zhu, G.; Pfeifer, J.; Bax, A. *J. Biomol. NMR* **1995**, *6*, 277–293.

(25) Kamith, U.; Shriver, J. W. *J. Biol. Chem.* **1989**, *264*, 5586–5592.

(26) Jacobsen, J. P.; Bildsoe, H. K.; Schaumburg, K. *J. Magn. Reson.* **1976**, *23*, 153–164.

(27) Mittermaier, A.; Kay, L. E. *J. Am. Chem. Soc.* **1999**, *121*, 10608–10613.

(28) Lipari, G.; Szabo, A. *J. Am. Chem. Soc.* **1982**, *104*, 4559–4570.

(29) Woessner, D. E. *J. Chem. Phys.* **1962**, *37*, 647–654.

D<sub>2</sub>O since they were initially prepared with other experiments in mind. There are, however, certain advantages in using samples dissolved in D<sub>2</sub>O; the absence of backbone amides eliminates cross relaxation between methyl groups and neighboring amide protons, leading to improvements in sensitivity and resolution in the TROSY-based schemes of Figure 2. One disadvantage is that the viscosity of D<sub>2</sub>O is on the order of 20% larger than H<sub>2</sub>O,<sup>30</sup> increasing the protein correlation time and hence the relaxation rates of the attached spins. This, of course, has detrimental effects for the quality of spectra. The rotational diffusion tensor for MSG in D<sub>2</sub>O was estimated as follows. First, single-field (600 MHz) <sup>15</sup>N relaxation data ( $R_{1\rho}$ ,  $R_1$ , and <sup>1</sup>H-<sup>15</sup>N NOEs) measured on a U-[<sup>15</sup>N,<sup>2</sup>H] Ile $\delta$ 1-[<sup>13</sup>CH<sub>3</sub>] Leu,Val-[<sup>13</sup>CH<sub>3</sub>,<sup>12</sup>CD<sub>3</sub>]-labeled sample in H<sub>2</sub>O (see earlier discussion) were obtained using TROSY-based<sup>31</sup> pulse schemes. A standard analysis of these <sup>15</sup>N data,<sup>32,33</sup> assuming average values for ( $S_{\text{NH}}^2$ ;  $\tau_e$ ) of (0.85; 20ps) and selecting only residues from regular secondary structure with NOE values > 0.6, gives  $\tau_{\text{c,eff}} = 39.2 \pm 0.1$  ns and diffusion anisotropy,  $D_{\parallel}/D_{\perp}$ , of  $1.21 \pm 0.03$  (with polar angles  $\theta = 13 \pm 4^\circ$  and  $\phi = 48 \pm 17^\circ$  describing the orientation of the unique diffusion axis relative to the molecular inertia coordinate frame). F-test analysis<sup>34</sup> showed that the axially symmetric model represents a statistically significant improvement over the isotropic model and that more complex models than axially symmetric cannot be justified. The diffusion parameters listed above are used as a reference for estimation of rotational correlation time(s) in D<sub>2</sub>O. Second, the translational diffusion constant ( $D'$ ) for this sample was determined using a two-dimensional NMR experiment that has been described previously that measures diffusion at each methyl position in the protein.<sup>35</sup> In a third step, the translational diffusion experiments were repeated on the D<sub>2</sub>O samples to obtain diffusion constants for each sample and the respective rotational correlation times were calculated directly as  $\tau_{\text{c,eff}}(\text{sample in D}_2\text{O}) = [D'(\text{reference sample in H}_2\text{O})/D'(\text{sample in D}_2\text{O})] \times \tau_{\text{c,eff}}(\text{reference sample in H}_2\text{O})$ . In this manner, values of  $\tau_{\text{c,eff}}$  of 56 and 54 ns were determined for Ile $\delta$ 1-[<sup>13</sup>CH<sub>2</sub>D]-MSG and Ile $\delta$ 1-[<sup>13</sup>CHD<sub>2</sub>]-MSG samples, respectively.

To establish the validity of the relation between translational and rotational diffusion above, we have carried out a series of experiments on an Ile $\delta$ 1-[<sup>13</sup>CH<sub>3</sub>]-labeled sample of MSG in D<sub>2</sub>O as a function of protein concentration in the range between ~0.3 and ~0.8 mM (~24 to ~66 mg/mL). Diffusion constants were measured in each case along with <sup>1</sup>H-<sup>13</sup>C multiple-quantum (MQ) relaxation rates<sup>21</sup> that are proportional to  $\tau_{\text{c,eff}}(\text{D}_2\text{O})$ . Notably, both  $1/\tau_{\text{c,eff}}$  and  $D'$  decreased with increasing protein content, consistent with the solution viscosity depending on protein concentration, as has been observed for a number of other proteins.<sup>36–38</sup> Moreover, at each dilution point the MQ relaxation times scaled on average exactly as the translational diffusion constants, in very strong support of the relation above linking  $\tau_{\text{c,eff}}(\text{sample, D}_2\text{O})$  and  $\tau_{\text{c,eff}}(\text{reference, H}_2\text{O})$  and suggesting that for MSG both translational and rotational properties scale with viscosity in the same manner, over the concentration range examined.

## Results and Discussion

**Labeling Strategy.** Previously, our laboratory has introduced a set of <sup>2</sup>H-based relaxation experiments for the study of methyl

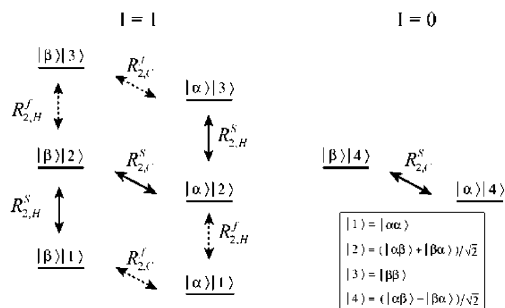
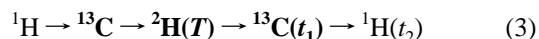


**Figure 1.** Energy level diagram for the <sup>13</sup>CH<sub>2</sub> spin system of a rapidly rotating <sup>13</sup>CH<sub>2</sub>D methyl group. Two manifolds are illustrated although only one ( $I = 1$ ) contributes to signal in the experiments described in the text. Slow (fast) relaxing <sup>13</sup>C-<sup>1</sup>H transitions are shown with solid (dashed) arrows. A product basis representation of each eigenfunction is used,  $|j\rangle|k\rangle$ , where  $j = \{\alpha, \beta\}$  is the <sup>13</sup>C spin state and  $k = \{1, 2, 3, 4\}$  is the wave function for the pair of magnetically equivalent <sup>1</sup>H spins. Expressions for the relaxation rates are given in the text.

side-chain dynamics in small, uniformly <sup>13</sup>C, ~50% fractionally deuterated proteins.<sup>13,15</sup> In these experiments, <sup>13</sup>CH<sub>2</sub>D methyl isotopomers are selected from the set of <sup>13</sup>CH<sub>3</sub>, <sup>13</sup>CH<sub>2</sub>D, <sup>13</sup>CHD<sub>2</sub>, and <sup>13</sup>CD<sub>3</sub> methyl groups that are present in a fractionally deuterated protein. The use of fractionally deuterated samples is advantageous in that methyl groups from all methyl-containing amino acids are accessible. However, a disadvantage is that the population of the targeted <sup>13</sup>CH<sub>2</sub>D isotopomer is very much reduced. Recent advances in labeling approaches allow the complete incorporation of the isotopomer of choice into Ile, Leu, and Val methyl positions,<sup>21,39,40</sup> leading to significant increases in sensitivity. In the present study, samples were prepared in which Ile  $\delta$ 1 positions are either <sup>13</sup>CH<sub>2</sub>D- or <sup>13</sup>CHD<sub>2</sub>-labeled, through the addition of appropriate biosynthetic precursors described in the Materials and Methods section. All other carbon positions in the protein are <sup>12</sup>C so that delay elements in pulse schemes can be chosen without concern about evolution due to <sup>13</sup>C-<sup>13</sup>C one-bond scalar couplings, leading again to improvements in sensitivity (see later discussion).

**Important Considerations in the Design of <sup>2</sup>H Relaxation Experiments.** Deuterium relaxation can be measured using an experiment in which the magnetization flow is described as



where the transfer from one spin to the next is achieved via one-bond scalar couplings and  $t_1, t_2$  are acquisition times. A series of two-dimensional [<sup>1</sup>H, <sup>13</sup>C] correlation maps are obtained as a function of time  $T$ , with the intensity of peaks related directly to the <sup>2</sup>H relaxation rate. The <sup>2</sup>H spin relaxation experiments that have been described to date<sup>13,15</sup> are all based on HSQC schemes;<sup>41</sup> for applications involving very high molecular weight proteins such sequences become particularly inefficient.

To understand why the quality of HSQC-type magnetization transfer schemes degrade rapidly with molecular weight, we focus initially on the energy level diagram for a <sup>13</sup>CH<sub>2</sub>D methyl (Figure 1). For simplicity, the deuteron is considered as a “silent” spin for the moment, so that the energy levels of the methyl coincide with those of an AX<sub>2</sub> spin system ( $A = ^{13}\text{C}$ ,  $X = ^1\text{H}$ ),

- (30) Cho, C. H.; Urquidí, J.; Singh, S.; Robinson, G. W. *J. Phys. Chem. B* **1999**, *103*, 1991–1994.  
 (31) Pervushin, K.; Riek, R.; Wider, G.; Wüthrich, K. *Proc. Natl. Acad. Sci. U.S.A.* **1997**, *94*, 12366–12371.  
 (32) Tjandra, N.; Feller, S. E.; Pastor, R. W.; Bax, A. *J. Am. Chem. Soc.* **1995**, *117*, 12562–12566.  
 (33) Lee, L. K.; Rance, M.; Chazin, W. J.; Palmer, A. G. *J. Biomol. NMR* **1997**, *9*, 287–298.  
 (34) Bevington, P. R.; Robinson, D. K. *Data Reduction and Error Analysis for the Physical Sciences*; WCB/McGraw-Hill: New York, 1992.  
 (35) Choy, W. Y.; Mulder, F. A. A.; Crowhurst, K. A.; Muhandiram, D. R.; Millett, I. S.; Doniach, S.; Forman-Kay, J. D.; Kay, L. E. *J. Mol. Biol.* **2002**, *316*, 101–112.  
 (36) Iino, M.; Okuda, Y. *Jpn. J. Appl. Phys.* **1997**, *36*, 3786–3790.  
 (37) Damberg, P.; Jarvet, J.; Allard, P.; Mets, U.; Rigler, R.; Gräslund, A. *Biophys. J.* **2002**, *83*, 2812–2825.  
 (38) Monkos, K. *Biochim. Biophys. Acta* **2004**, *1700*, 27–34.

- (39) Goto, N. K.; Gardner, K. H.; Mueller, G. A.; Willis, R. C.; Kay, L. E. *J. Biomol. NMR* **1999**, *13*, 369–374.  
 (40) Tugarinov, V.; Hwang, P. M.; Kay, L. E. *Annu. Rev. Biochem.* **2004**, *73*, 107–146.  
 (41) Bodenhausen, G.; Rubin, D. J. *Chem. Phys. Lett.* **1980**, *69*, 185–189.

and only the relaxation contributions from dipolar interactions involving methyl  $^1\text{H}$  and  $^{13}\text{C}$  spins are considered. Transitions within the  $I = 1$  manifold only are of issue in what follows since the  $I = 0$  manifold is not accessed in an HSQC experiment. Notably, calculations establish that for  $^{13}\text{CH}_2\text{D}$  methyl groups attached to large proteins the relaxation of individual  $^1\text{H}$  and  $^{13}\text{C}$  transitions is single exponential in the limit of very rapid rotation of the methyl about its symmetry axis and in the absence of relaxation contributions from external spins. Moreover, individual transitions can relax very differently due to interference effects between the different dipolar fields within the  $^{13}\text{CH}_2\text{D}$  methyl. For example, with the assumptions given earlier, the relaxation rates  $R_{2,\text{H}}^f$  and  $R_{2,\text{H}}^s$  of the  $^1\text{H}$  transitions (vertical lines) are

$$R_{2,\text{H}}^f = \left(\frac{1}{45}\right) \frac{S_{\text{axis}}^2 \gamma_{\text{C}}^2 \gamma_{\text{H}}^2 \hbar^2 \tau_{\text{C}}}{r_{\text{CH}}^6} + \left(\frac{9}{80}\right) \frac{S_{\text{axis}}^2 \gamma_{\text{H}}^4 \hbar^2 \tau_{\text{C}}}{r_{\text{HH}}^6} + \left(\frac{1}{10}\right) \frac{S_{\text{axis}}^2 \gamma_{\text{C}} \gamma_{\text{H}}^3 \hbar^2 \tau_{\text{C}}}{r_{\text{CH}}^3 r_{\text{HH}}^3} \quad (4a)$$

$$R_{2,\text{H}}^s = \left(\frac{1}{45}\right) \frac{S_{\text{axis}}^2 \gamma_{\text{C}}^2 \gamma_{\text{H}}^2 \hbar^2 \tau_{\text{C}}}{r_{\text{CH}}^6} + \left(\frac{9}{80}\right) \frac{S_{\text{axis}}^2 \gamma_{\text{H}}^4 \hbar^2 \tau_{\text{C}}}{r_{\text{HH}}^6} - \left(\frac{1}{10}\right) \frac{S_{\text{axis}}^2 \gamma_{\text{C}} \gamma_{\text{H}}^3 \hbar^2 \tau_{\text{C}}}{r_{\text{CH}}^3 r_{\text{HH}}^3} \quad (4b)$$

where  $r_{ij}$  is the distance between spins  $i$  and  $j$ ,  $\gamma_i$  is the gyromagnetic ratio of spin  $i$ , and only those contributions proportional to the overall (assumed isotropic) correlation time,  $\tau_{\text{C}}$ , have been included. Terms 1, 2, and 3 in the expressions above include (auto- and cross-correlation) contributions from intramethyl  $^1\text{H}-^{13}\text{C}$ ,  $^1\text{H}-^1\text{H}$  and  $^1\text{H}-^{13}\text{C}, ^1\text{H}-^1\text{H}$  dipolar interactions, respectively. The partial cancellation of local fields for the slowly relaxing  $^1\text{H}$  transitions derives from a TROSY<sup>31</sup> effect that is dipolar in origin, similar to that described previously in the context of methyl-TROSY spectroscopy.<sup>20,42</sup> The effect can be considerable; calculated values for  $R_{2,\text{H}}^f$  and  $R_{2,\text{H}}^s$  are 144 and 24  $\text{s}^{-1}$  (using experimental dynamics parameters for Ile- $^{13}\text{CH}_2\text{D}$ -MSG of  $\tau_{\text{C}} = 56$  ns,  $S_{\text{axis}}^2 = 0.6$ ), in reasonable agreement with average measured values of 127.2 and 34.0  $\text{s}^{-1}$ . As a result, each line of a  $^{13}\text{C}$ -coupled  $^1\text{H}$  doublet consists of fast and slow relaxing components that, apart from a very small dynamic frequency shift, are degenerate.

Similar to the  $^1\text{H}$  lines, the  $^{13}\text{C}$  transitions (indicated by horizontal lines, Figure 1) can also relax very differently, as described previously in the context of  $\text{AX}_2$  spin systems by Prestegard and Grant.<sup>43</sup> A straightforward calculation using the above-mentioned assumptions shows that  $R_{2,\text{C}}^f$  and  $R_{2,\text{C}}^s$  are given by:

$$R_{2,\text{C}}^f = \left(\frac{4}{45}\right) \frac{S_{\text{axis}}^2 \gamma_{\text{C}}^2 \gamma_{\text{H}}^2 \hbar^2 \tau_{\text{C}}}{r_{\text{CH}}^6} \quad (5a)$$

$$R_{2,\text{C}}^s = 0 \quad (5b)$$

$R_{2,\text{C}}^f$  is calculated to be approximately 50  $\text{s}^{-1}$ , close to the average value measured for Ile  $\delta 1$  positions ( $^{13}\text{CH}_2\text{D}$ ) in MSG, 52.1  $\text{s}^{-1}$ . An average value of 13.6  $\text{s}^{-1}$  was obtained for  $R_{2,\text{C}}^s$  in MSG that is largely the result of contributions from spins external to the methyl groups in question. Thus, the  $^{13}\text{C}$  direct observe,  $^2\text{H}$ -decoupled spectrum of a  $^{13}\text{CH}_2\text{D}$  methyl comprises a triplet, with a narrow inner line flanked by two broad outer resonances. A very similar situation occurs when the HMQC scheme<sup>44,45</sup> is applied to  $^{13}\text{CH}_3$  groups and gives rise to a methyl-TROSY effect that our group has exploited in studies of high molecular weight proteins.<sup>20,42</sup> It is worth noting that the relaxation pattern observed for the lines in  $^{13}\text{C}$  spectra of  $^{13}\text{CH}_2\text{D}$  groups is in contrast to the profile in spectra of "static" methylenes where the outer lines relax more slowly.<sup>14,46</sup> In this case, it is also possible to develop  $^{13}\text{CH}_2$ -TROSY experiments, as has recently been demonstrated by Miclet et al.<sup>46</sup>

To maximize sensitivity and resolution in spectra of  $^{13}\text{CH}_2\text{D}$  methyls, it is important to design  $^{13}\text{CH}_2\text{D}$ -TROSY experiments in which signal derives principally from transitions that relax slowly. This situation, unfortunately, does not occur in HSQC-type experiments, leading to significant losses in both sensitivity and resolution in applications that involve very high molecular weight proteins. Central to the HSQC scheme are INEPT magnetization transfer elements<sup>47</sup> that in the case of a  $^{13}\text{CH}_2$  group transfer magnetization from protons to the outer carbon lines of the carbon triplet, denoted by the dashed horizontal arrows in Figure 1. As described above, these outer lines relax very rapidly, degrading resolution in the  $^{13}\text{C}$  dimension of  $^1\text{H}, ^{13}\text{C}$  correlation maps, and in the case of  $^2\text{H}$  relaxation experiments, also sensitivity since subsequent transfer steps (such as the  $^{13}\text{C}$  to  $^2\text{H}$  transfers, indicated in bold in eq 3) become inefficient. In addition, the  $^{13}\text{C}$  decoupling typically used during acquisition in HSQC experiments leads to a mixing of rapid and slowly relaxing proton lines (denoted by dashed and solid vertical arrows in Figure 1), further reducing the quality of spectra (see later discussion).

The above discussion suggests that an optimal  $^1\text{H}, ^{13}\text{C}$  correlation experiment for  $^{13}\text{CH}_2\text{D}$  methyl groups is one where magnetization is transferred with maximum efficiency to the central (slowly relaxing)  $^{13}\text{C}$  line and then subsequently to  $^2\text{H}$ . Because the relaxation of magnetization proceeds with a rate of  $R_{2,\text{C}}^f$ , rather than  $R_{2,\text{C}}^s$ , as is the case in the standard HSQC experiment, the sensitivity can be significantly improved in applications to large proteins (see later discussion). To further optimize sensitivity, it is desirable to transfer magnetization back from  $^{13}\text{C}$  to the slowly relaxing proton transitions and to ensure that fast and slowly relaxing lines are not interchanged during detection. In what follows such a pulse scheme is described.

**Pulse Schemes for the Measurement of  $^2\text{H}$  Relaxation in  $^{13}\text{CH}_2\text{D}$  Methyl Groups.** Figure 2 shows the sequence that has been developed for the measurement of the relaxation of the  $^2\text{H}$  density elements,  $D_+$  (A),  $D_z$  (B),  $D_+D_z + D_zD_+$  (C) and  $3D_z^2 - 2$  (D), where  $D_+ = D_x + iD_y$ , and  $D_x, D_y, D_z$  are the  $x, y, z$  components of deuterium magnetization. In what follows below, a brief description of the pulse scheme is provided using

(44) Mueller, L. *J. Am. Chem. Soc.* **1979**, *101*, 4481–4484.

(45) Bax, A.; Griffey, R. H.; Hawkins, B. L. *J. Magn. Reson.* **1983**, *55*, 301–315.

(46) Miclet, E.; Williams, D. C., Jr.; Clore, G. M.; Bryce, D. L.; Boisbouvier, J.; Bax, A. *J. Am. Chem. Soc.* **2004**, *126*, 10560–10570.

(47) Morris, G. A.; Freeman, R. *J. Am. Chem. Soc.* **1979**, *101*, 760–762.

(42) Ollerenshaw, J. E.; Tugarinov, V.; Kay, L. E. *Magn. Reson. Chem.* **2003**, *41*, 843–852.

(43) Prestegard, J. H.; Grant, D. M. *J. Am. Chem. Soc.* **1978**, *100*, 4664–4668.

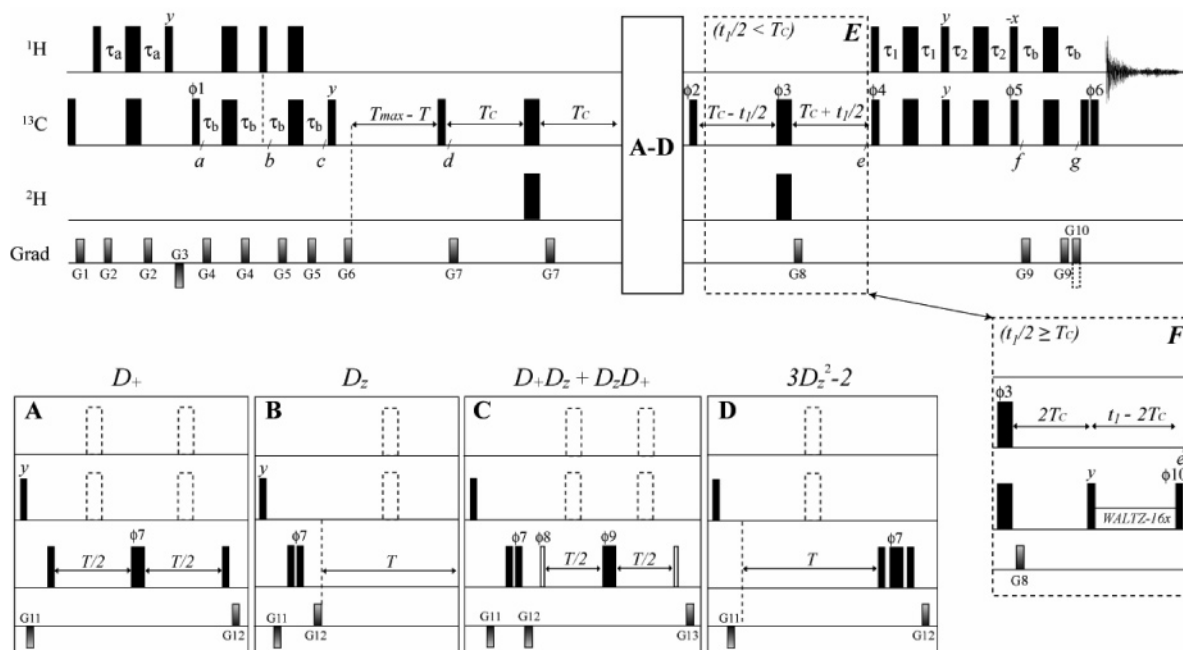


**Figure 2.** CH<sub>2</sub>D-TROSY pulse scheme for <sup>2</sup>H relaxation measurements in <sup>13</sup>CH<sub>2</sub>D methyl groups. All narrow (wide) rectangular pulses are applied with flip angles of 90 (180)° along the *x*-axis unless indicated otherwise. The <sup>1</sup>H, <sup>2</sup>H, and <sup>13</sup>C carrier frequencies are positioned in the center of the Ileδ1 methyl region at 1, 1, and 12 ppm, respectively. All <sup>1</sup>H and <sup>13</sup>C pulses are applied with the highest possible power, while a 2-kHz field is used for <sup>2</sup>H pulses. Blocks A–D are inserted into the pulse scheme for the measurement of the relaxation of *D*<sub>+</sub> (A), *D*<sub>z</sub> (B), *D*<sub>+</sub>*D*<sub>z</sub> + *D*<sub>z</sub>*D*<sub>+</sub> (C), and *3D*<sub>z</sub><sup>2</sup> – 2 (D).<sup>15</sup> The narrow pulses in block C shown as open rectangles have flip angles of 45°. The dashed 180° pulses during relaxation delays *T* are optional (see text). Delays are:  $\tau_a = 1.8$  ms;  $\tau_b = 1$  ms;  $2\tau_1 = 1.33$  ms; and  $2\tau_2 = 1.57$  ms;  $T_C = 6.25$  (12.0) ms for schemes in insets A, B (C, D) (see text). For  $t_1 \geq 2T_C$ , scheme E is replaced by F with WALTZ-16 <sup>2</sup>H decoupling<sup>48</sup> achieved using a 0.5-kHz field. The durations and strengths of the *z*-gradients in units of (ms; G/cm) are: G1 = (1; 7.5), G2 = (0.5; 10), G3 = (1; –8), G4 = (0.2; 6), G5 = (0.5; 18), G6 = (1; 20), G7 = (0.3; 12), G8 = (0.5; 30), G9 = (0.2; 25), G10 = (0.125; 29.5), G11 = (0.3; –15), G12 = (0.3; 7) (insets A, B, D), G12 = (0.3; –15) (inset C), G13 = (0.3; 7). The phase cycle is:  $\phi_1 = x, -x$ ;  $\phi_2 = y$  (insets A, B),  $\phi_2 = x$  (insets C, D);  $\phi_3 = 4(x), 4(y), 4(-x), 4(-y)$ ;  $\phi_4 = x, -x$ ;  $\phi_5 = -x$ ;  $\phi_6 = -x$ ;  $\phi_7 = 2(x), 2(y), 2(-x), 2(-y)$  (inset A),  $\phi_7 = 2(x), 2(-x)$  (inset B),  $\phi_7 = 4(x), 4(-x)$  (inset C),  $\phi_7 = 2(0^\circ), 2(45^\circ), 2(90^\circ), 2(135^\circ)$  (inset D);  $\phi_8 = 8(x), 8(-x)$ ;  $\phi_9 = x, -x, y, -y$ ;  $\phi_{10} = -y, -y, y, y$  (insets A, C, D),  $\phi_{10} = y, y, -y, -y$  (inset B); rec = *x, -x, -x, x, -x, x, x, -x* (insets A, B, D), rec = *x, -x, -x, x, 2(-x, x, x, -x), x, -x, -x, x* (inset C). Quadrature detection in *F*<sub>1</sub> is achieved via a gradient-enhanced sensitivity scheme where for each *t*<sub>1</sub> value a pair of spectra are recorded with  $\phi_4 = x$ ; G10 and  $\phi_4 = -x$ ; –G10 and manipulated postacquisition.<sup>49,50</sup> The phase  $\phi_2$  is inverted for each *t*<sub>1</sub> point.<sup>51</sup> Two data sets are recorded with  $\phi_5, \phi_6$  as indicated above and with  $\phi_5, \phi_6$  simultaneously inverted and manipulated as described in the text to obtain singlets in *F*<sub>2</sub>.

a notation in which the contributions to the density operator from individual transitions are made clear since, as described earlier, such lines can relax very differently. Thus, *y*-transverse magnetization from the fast (slowly) relaxing <sup>13</sup>C lines is denoted by  $C_y|1\rangle\langle 1|, C_y|3\rangle\langle 3|, (C_y|2\rangle\langle 2|)$ . Multiplicative factors that precede the density terms are generally ignored. At point *a* in the pulse scheme of Figure 2 the magnetization of interest is given by  $2C_y(|1\rangle\langle 1| - |3\rangle\langle 3|)$ , so that only the outer <sup>13</sup>C lines that relax rapidly (Figure 1) are effectively “excited”. During a subsequent delay of  $2\tau_b = 1/(4^1J_{CH})$ , the magnetization evolves to  $2C_x(|1\rangle\langle 1| + |3\rangle\langle 3|)$  and following the application of a <sup>1</sup>H 90° pulse the density operator at point *b* is given by  $C_x(|1\rangle\langle 1| + |3\rangle\langle 3| + 2|2\rangle\langle 2| - |1\rangle\langle 3| - |3\rangle\langle 1|)$ . Thus, a significant fraction of the magnetization is transferred to the central <sup>13</sup>C transition at this point, corresponding to  $1/\sqrt{2}$  of the starting proton polarization, which relaxes much more slowly in large proteins than the outer <sup>13</sup>C components (see above discussion). During the subsequent period extending from *b* to *c* the outer lines,  $C_x(|1\rangle\langle 1| + |3\rangle\langle 3|)$ , evolve due to <sup>1</sup>*J*<sub>CH</sub> while the central line does not, so that at point *c* the following elements are present:  $C_y(|1\rangle\langle 1| - |3\rangle\langle 3|) + C_x(2|2\rangle\langle 2| - |1\rangle\langle 3| - |3\rangle\langle 1|)$ . The subsequent application of a <sup>13</sup>C *y*-pulse and a gradient (G6) eliminates both the outer lines (terms proportional to *C*<sub>*y*</sub>) and the double-quantum terms, leaving the slowly decaying magnetization of interest,  $2C_z|2\rangle\langle 2|$ , which relaxes during the delay  $T_{max} - T$  (see later discussion). During the subsequent delay,

$2T_C$ , the central line evolves due to the carbon–deuteron one-bond scalar coupling, <sup>1</sup>*J*<sub>CD</sub> (~20 Hz), and depending on which <sup>2</sup>H relaxation rate is measured, blocks A–D of Figure 2 are selected, with  $2T_C$  adjusted to  $\sim 1/(4^1J_{CD})$  for the measurement of  $R^Q(D_+)$  and  $R^Q(D_z)$ , as described by Muhandiram et al.,<sup>13</sup> and to  $\sim 1/(2^1J_{CD})$  for the measurement of  $R^Q(D_+D_z + D_zD_+)$ ,  $R^Q(3D_z^2 - 2)$ , according to Millet et al.<sup>15</sup> Note that there is no need to adjust  $2T_C$  to a multiple of  $(1/^1J_{CC})$ , as the Ile side chains are selectively <sup>13</sup>C-labeled at only the δ1 positions. During the delay, *T*, magnetization of the form  $2C_z|2\rangle\langle 2|[D]$  relaxes, where *[D]* corresponds to the <sup>2</sup>H operator of interest (*D*<sub>+</sub>, *D*<sub>z</sub>, *D*<sub>+</sub>*D*<sub>z</sub> + *D*<sub>z</sub>*D*<sub>+</sub>, *3D*<sub>z</sub><sup>2</sup> – 2). Subsequently, magnetization is refocused with respect to <sup>2</sup>H during the second  $2T_C$  period and labeled with <sup>13</sup>C chemical shift. To achieve better resolution in *F*<sub>1</sub>, the pulse sequence is extended with a nonconstant time acquisition period (with <sup>2</sup>H-decoupling) in the case where  $t_{1/2} \geq T_C$ . Finally, magnetization is transferred from the central <sup>13</sup>C transition,  $2C_y|2\rangle\langle 2|$ , to the slow-relaxing <sup>1</sup>H transitions in a manner that preserves both cosine and sine modulated *t*<sub>1</sub> components using a pulse module very similar to a regular sensitivity enhancement scheme<sup>52</sup> and to the planar TOCSY element proposed by Ernst

(48) Shaka, A. J.; Keeler, J.; Frenkiel, T.; Freeman, R. J. *Magn. Reson.* **1983**, *52*, 335–338.

(49) Kay, L. E.; Keifer, P.; Saarinen, T. *J. Am. Chem. Soc.* **1992**, *114*, 10663–10665.

(50) Schleucher, J.; Sattler, M.; Griesinger, C. *Angew. Chem., Int. Ed.* **1993**, *32*, 1489–1491.

and co-workers.<sup>53,54</sup> Between points *e* and *f* of the pulse scheme,  $2C_y|2\rangle\langle 2|$  is transferred to

$$C_z(H_{y,1} + H_{y,2}) \cos^2(2\pi J_{CH}\tau_1) \sin(4\pi J_{CH}\tau_2) - (H_{y,1}H_{z,2} + H_{z,1}H_{y,2}) \sin(4\pi J_{CH}\tau_1) \cos(2\pi J_{CH}\tau_2) \quad (6a)$$

while  $2C_x|2\rangle\langle 2|$  becomes

$$C_z(H_{x,1} + H_{x,2}) \sin(4\pi J_{CH}\tau_1) \cos(2\pi J_{CH}\tau_2) - (H_{x,1}H_{z,2} + H_{z,1}H_{x,2}) \cos^2(2\pi J_{CH}\tau_1) \sin(4\pi J_{CH}\tau_2) \quad (6b)$$

It is possible to show, based on Figure 1, that the magnetization from the slowly relaxing  $^1\text{H}$  lines can be written as  $C^\beta(|1\rangle\langle 2| + |2\rangle\langle 1|) + C^\alpha(|2\rangle\langle 3| + |3\rangle\langle 2|) = (1/\sqrt{2})[(H_{x,1} + H_{x,2}) - 4C_z(H_{x,1}H_{z,2} + H_{z,1}H_{x,2})]$  (in-phase) or as  $-C^\beta(|1\rangle\langle 2| + |2\rangle\langle 1|) + C^\alpha(|2\rangle\langle 3| + |3\rangle\langle 2|) = (1/\sqrt{2})[2C_z(H_{x,1} + H_{x,2}) - 2(H_{x,1}H_{z,2} + H_{z,1}H_{x,2})]$  (anti-phase). It is clear, therefore, that for a complete transfer between “long-lived” carbon and proton lines to occur the delays  $\tau_1$  and  $\tau_2$  (eq 6) must be chosen such that  $\sin(4\pi J_{CH}\tau_1) \cos(2\pi J_{CH}\tau_2) = \cos^2(2\pi J_{CH}\tau_1) \sin(4\pi J_{CH}\tau_2)$  (i.e.,  $\tan(2\pi J_{CH}\tau_1) = \sin(2\pi J_{CH}\tau_2)$ ), and that for an optimal transfer  $\tau_1, \tau_2$  must be set such that each of the trigonometric terms in the above expressions is maximized. This occurs for  $2\tau_1 = 1/(6J_{CH})$  and  $2\tau_2 = [\arcsin(\sqrt{3}/3)]/(\pi J_{CH})$ . The magnetization at point *f* is anti-phase with respect to the  $^{13}\text{C}$  spin; therefore, it is evolved with respect to  $J_{CH}$  for a period of  $2\tau_b = 1/(4J_{CH})$  to create a linear combination of in-phase and anti-phase terms at point *g* that are manipulated in a postacquisition manner to generate a “decoupled” spectrum. This is accomplished by recording data sets with (i)  $\phi_5 = \phi_6 = -x$  and with (ii)  $\phi_5, \phi_6$  simultaneously inverted. The addition and subtraction of these data sets, followed by a  $90^\circ$  phase correction in the acquisition dimension for one of the maps, and a subsequent addition/subtraction step yield two spectra with only one of the  $^1\text{H}-^{13}\text{C}$  doublet components in each. Subsequently, one spectrum is circular shifted by  $^1J_{CH}$  and added to the other to increase the signal-to-noise by  $\sqrt{2}$ . The uniformity of  $^1J_{CH}$  values in methyl groups (and especially in Ile residues)<sup>55</sup> makes this approach robust. It is worth noting, however, that while the addition of two separate spectra in this manner achieves “decoupling”, there is a cost of  $\sqrt{2}$  in sensitivity relative to a regular  $^{13}\text{C}$ -decoupled spectrum *if relaxation effects are ignored* (i.e., when  $R_{2,H}^s = R_{2,H}^f$ ). This disadvantage is, however, more than compensated for in applications to large proteins since traditional decoupling schemes would interconvert the slowly and fast relaxing  $^1\text{H}$  components, so that the detected  $^1\text{H}$  magnetization would relax with an effective rate of  $0.5(R_{2,H}^s + R_{2,H}^f)$  rather than as in the preferred scheme of Figure 2 where the rate is  $R_{2,H}^s$ . Figure 3 illustrates the postacquisition manipulations described earlier to produce spectra with singlet components for each Ile correlation.

As described earlier, it is the relaxation of  $2C_x|2\rangle\langle 2|[D]$  that is measured during *T*, as opposed to  $[D]$ . This is the case in our

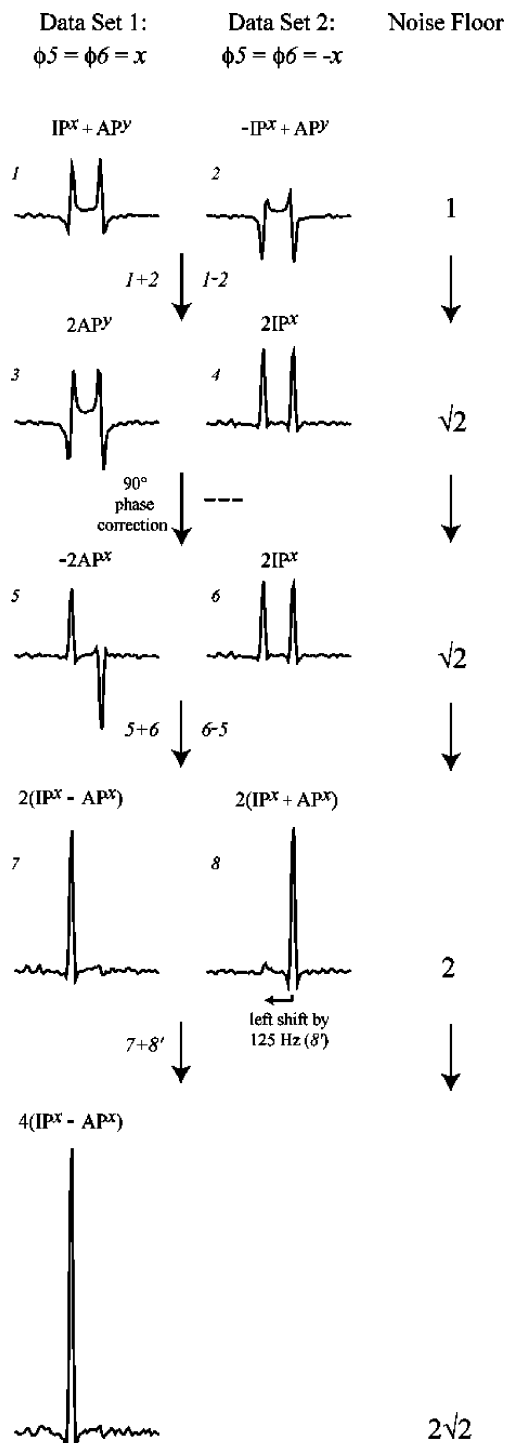


**Figure 3.** Postacquisition manipulations of data recorded with the pulse scheme of Figure 2 to generate pure absorptive singlet components for each methyl correlation.  $\text{IP}^x$  and  $\text{AP}^x$  are defined as  $\text{IP}^x = (1/\sqrt{2})[(H_{x,1} + H_{x,2}) - 4C_z(H_{x,1}H_{z,2} + H_{z,1}H_{x,2})]$ ,  $\text{AP}^x = (1/\sqrt{2})[2C_z(H_{x,1} + H_{x,2}) - 2(H_{x,1}H_{z,2} + H_{z,1}H_{x,2})]$ , while  $\text{IP}(\text{AP})^y$  is obtained from  $\text{IP}(\text{AP})^x$  by replacing  $H_x$  with  $H_y$ . Manipulations of data sets 1 and 2 via  $1 + 2$ ,  $1 - 2$ ,  $90^\circ$  phase correction, generates in-phase and anti-phase multiplet components that can subsequently be combined ( $5 + 6$ ,  $6 - 5$ ,  $7 + 8'$ ) to generate spectra with only a single “decoupled” component that has a factor of 2 increase in signal-to-noise (s/n) relative to the corresponding (downfield) components in either 5 or 6. The net effect is to produce a spectrum with correlations that are reduced by a factor of  $\sqrt{2}$  in s/n relative to those in a fully decoupled correlation map (obtained with a slightly modified sequence derived from the scheme of Figure 2), neglecting relaxation. As described in the text, in applications to large proteins relaxation cannot be ignored, and the approach above (eliminating decoupling) generates spectra of significantly improved resolution.

(51) Marion, D.; Ikura, M.; Tschudin, R.; Bax, A. *J. Magn. Reson.* **1989**, *85*, 393–399.

(52) Palmer, A. G.; Cavanagh, J.; Wright, P. E.; Rance, M. *J. Magn. Reson.* **1991**, *93*, 151–170.

(53) Mádi, Z. L.; Brutscher, B.; Schulte-Herbrüggen, T.; Brüschweiler, R.; Ernst, R. R. *Chem. Phys. Lett.* **1997**, *268*, 300–305.

(54) Schulte-Herbrüggen, T.; Mádi, Z. L.; Sørensen, O. W.; Ernst, R. R. *Mol. Phys.* **1991**, *72*, 847–853.

(55) Mittermaier, A.; Kay, L. E. *J. Biomol. NMR* **2002**, *23*, 35–45.

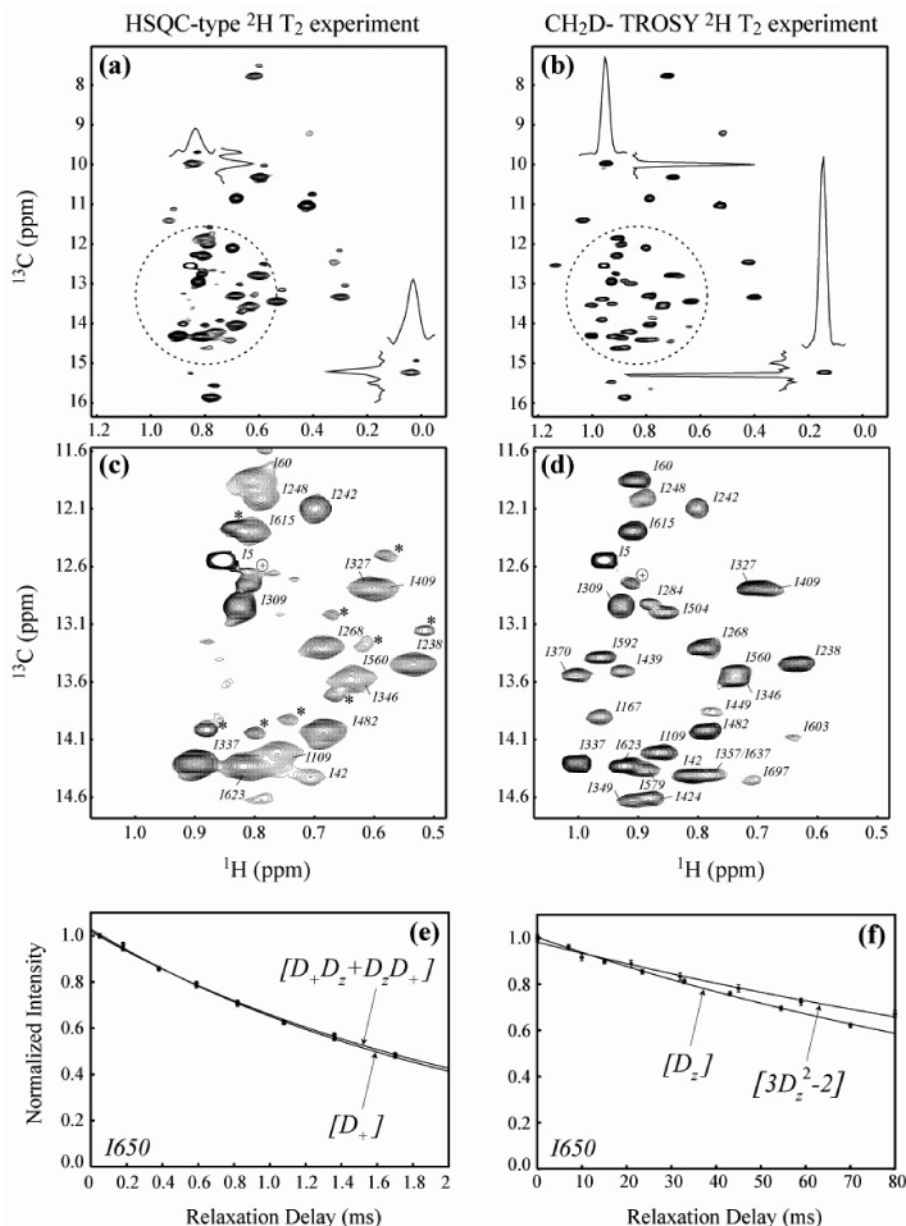


**Figure 4.** Comparison of (a,c) HSQC-based spectra<sup>13</sup> for measuring  $^2\text{H}$  relaxation rates ( $T = 0$  point of  $R^Q(D_+)$  measurement) and (b,d)  $\text{CH}_2\text{D}$ -TROSY correlation maps obtained with the pulse scheme of Figure 2 (panel a) recorded on an Ile $\delta$ 1- $^{13}\text{CH}_2\text{D}$ -labeled sample of MSG (37 °C, 600 MHz). The noise floors in each spectrum are normalized by dividing the  $\text{CH}_2\text{D}$ -TROSY data set by  $2\sqrt{2}$ , and the spectra are plotted at the same contour levels. The factor of  $2\sqrt{2}$  takes into account the increased noise floor in the  $\text{CH}_2\text{D}$ -TROSY spectrum that results from (i) the postacquisition manipulations that are used to generate singlets in  $F_2$  (Figure 3) and (ii) the enhanced sensitivity scheme for  $F_1$  quadrature detection that is used for the TROSY experiment that increases the noise floor by  $\sqrt{2}$  (and the signal by a factor of 2) relative to the HSQC data set. The regions indicated by the dashed circle in (a,b) are enlarged in panels (c,d). The peaks marked with asterisks in panel (c) belong to a  $^{13}\text{CHD}_2$  isotopic impurity in the Ile $\delta$ 1- $^{13}\text{CH}_2\text{D}$ -labeled sample that originates from the precursor (see Materials and Methods). The peaks marked with  $\oplus$  in panels (c,d) belong to a second conformation of Ile 309. (e,f) Relaxation decay curves for measurement of (e)  $R^Q(D_+)$  and  $R^Q(D_+D_z + D_zD_+)$  and (f)  $R^Q(D_z)$  and  $R^Q(3D_z^2 - 2)$  for Ile 650 $\delta$ 1 ( $^{13}\text{CH}_2\text{D}$  probe).

previously published experiments for studies of smaller proteins as well,<sup>13–15</sup> except that the decay rate of  $(H_{z,1} + H_{z,2})C_z[D]$  or  $C_z[D]$  is obtained. In the present case, the contribution to the relaxation of  $2C_z|2\rangle\langle 2|[D]$  from  $2C_z|2\rangle\langle 2|$  is subtracted “on the fly” by including the element of duration  $T_{\text{max}} - T$ , similar to an approach used in sequences designed for smaller proteins.<sup>15</sup> Simulations that take into account all possible relaxation mechanisms including the contributions from external protons indicate that to excellent approximation (less than 0.5% error)  $R^Q([D]) = R(2C_z|2\rangle\langle 2|[D]) - R(2C_z|2\rangle\langle 2|)$ .

In addition to the four  $^2\text{H}$  density elements that can be measured with the schemes in Figure 2, there is a fifth

coherence,  $^2\text{H}$  double quantum,  $D_+^2$ , that can also be studied. As discussed previously,<sup>15</sup> the decay of  $D_+^2$  is complicated by the fact that, in addition to relaxation contributions from quadrupolar terms, there are also interactions involving the methyl deuteron with carbon and proton spins that are internal or external (in the case of protons) to the methyl group. Notably, in the macromolecular limit the quadrupolar contribution scales as  $1/\tau_c$  (eq 1e), while the dipolar terms increase linearly with  $\tau_c$ . For small proteins the quadrupolar interaction dominates (the relative contributions from quadrupolar and intramethyl dipolar terms are on the order of 10:1 for  $\tau_c = 10$  ns), but for proteins the size of MSG the dipolar terms can be at least as

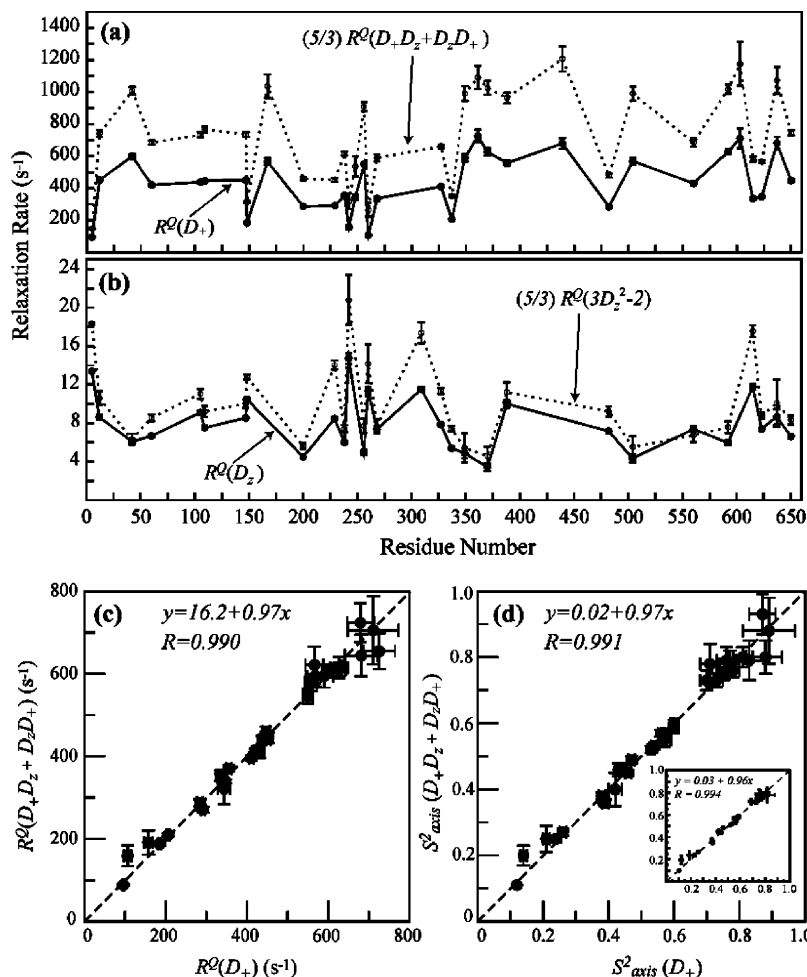


**Figure 5.** (a,b) All  $^2\text{H}$  relaxation data recorded for Ile $\delta 1$ - $^{13}\text{CH}_2\text{D}$  groups satisfy the inequality relation:  $(5/3)R^{\text{O}}(D_+D_z + D_zD_+) \geq R^{\text{O}}(D_+) \geq (5/3)R^{\text{O}}(3D_z^2 - 2) \geq R^{\text{O}}(D_z)$ . Linear correlation plots of (c)  $R^{\text{O}}(D_+D_z + D_zD_+)$  rates (y-axis) vs  $R^{\text{O}}(D_+)$  (x-axis) along with (d)  $R^{\text{O}}(D_+D_z + D_zD_+)$ -derived  $S^2_{\text{axis}}$  (y) vs  $R^{\text{O}}(D_+)$ -derived  $S^2_{\text{axis}}$  (x) for 33 Ile $\delta 1$ - $^{13}\text{CH}_2\text{D}$  peaks. Order parameters are extracted using eq 7 of the text. Best-fit parameters obtained from linear regression are indicated along with Pearson's correlation coefficients,  $R$ . The inset in (d) shows the correlation of  $S^2_{\text{axis}}$  values obtained by fitting rank 1 and rank 2 rates separately to the complete expressions for relaxation rates (eqs 1a–d, see text).

large as those due to the quadrupolar interaction. Correcting for such large contributions is error-prone, and we prefer, therefore, not to measure the decay of the double-quantum element.

In this section, we have discussed the advantages of the proposed pulse scheme in studies of high molecular weight proteins. These result from the fact that magnetization is “directed” along a pathway that minimizes relaxation losses and maximizes resolution, two important considerations in applications involving large systems. However, as in TROSY-based experiments for AX spin systems,<sup>31</sup> this manipulation comes at a price. A detailed analysis of the sequence of Figure 2, taking into account the postacquisition manipulations of Figure 3 as well, shows that, in the absence of relaxation and pulse imperfections,  $2\sqrt{2}$  in signal-to-noise is lost relative to the corresponding HSQC experiment. It is clear, therefore, that relaxation losses aside, HSQC-based experiments for measurement of  $^2\text{H}$  relaxation are preferred over those presented here. Computations using experimentally derived  $^1\text{H}$  and  $^{13}\text{C}$  relaxation rates suggest that the correlation time cutoff where the  $^{13}\text{CH}_2\text{D}$ -TROSY scheme becomes advantageous is approximately 25 ns, although it may be worth comparing pulse schemes in individual cases to ensure that the appropriate method is used.

**An Application to Ile- $\delta 1$   $^{13}\text{CH}_2\text{D}$  Methyls in MSG.** The pulse scheme of Figure 2 has been used to measure  $^2\text{H}$  relaxation rates at Ile  $\delta 1$  positions in MSG, with each Ile  $\delta 1$  labeled as “ $^{13}\text{CH}_2\text{D}$ ” using the appropriate precursors, as described in the Materials and Methods section. Figure 4a–d demonstrates the advantages of the new  $\text{CH}_2\text{D}$ -TROSY experiments relative to HSQC-based schemes.<sup>13,15</sup> The  $\text{CH}_2\text{D}$ -TROSY data set (Figure 4b,d) has been divided by  $2\sqrt{2}$  so that the noise floors are identical in each spectrum (note that the postacquisition processing of the TROSY data (Figure 3) increases the noise floor, relative to an HSQC data set). A gain in signal-to-noise of a factor of  $\sim 3$  has been achieved in a comparison of peak intensities in spectra obtained using the same acquisition parameters. The gain is reduced to an average factor of 2.2 if  $t_{1\text{max}}$  is limited to 40 ms (as opposed to 80 ms, see Materials and Methods section) in both experiments. It is clear that the line-narrowing in the  $^{13}\text{C}$ – $^1\text{H}$  dimensions and the concomitant gains in resolution are very substantial (Figure 4). Note that the peak positions in the  $\text{CH}_2\text{D}$ -TROSY experiment (Figure 4b,d) are shifted downfield in the  $^1\text{H}$  dimension by  $+^1J_{\text{CH}}/2$  Hz as a result of the processing procedure described earlier. Figure 4e,f shows typical exponential fits for the four  $^2\text{H}$  relaxation decay curves that have been obtained for Ile 650. In

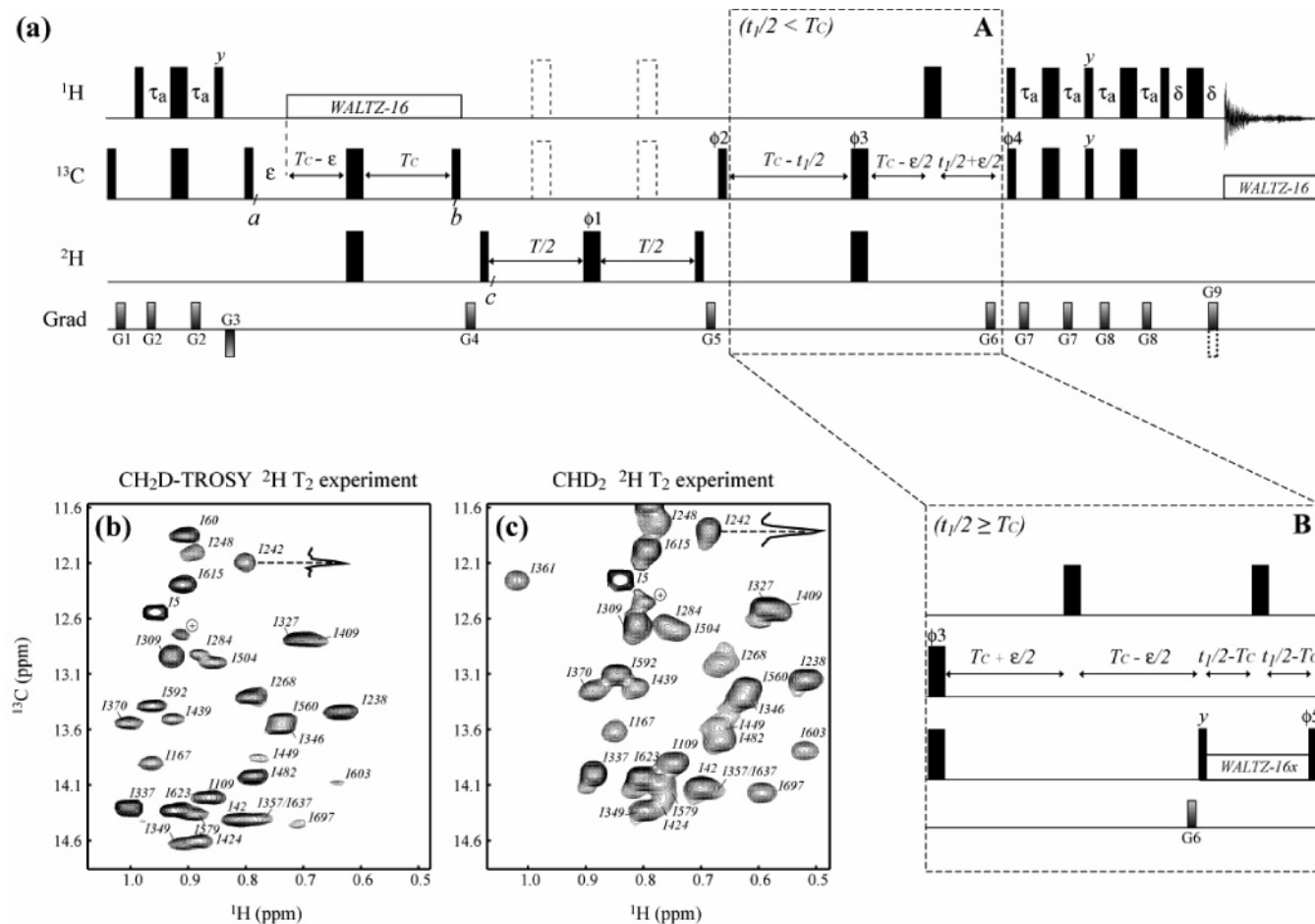


**Figure 6.** (a) Pulse scheme for the measurement of  $^2\text{H}$  transverse relaxation in  $^{13}\text{CHD}_2$ -labeled methyl groups in high molecular weight proteins. Some details of implementation are as in Figure 2.  $^{13}\text{C}$  and  $^1\text{H}$  WALTZ-16 decoupling<sup>48</sup> use 1.2 and 5.6 kHz fields, respectively. Delays are:  $\tau_a = 1.8$  ms;  $\epsilon = 4.0$  ms;  $\delta = 0.35$  ms;  $T_c = 4.0$  ms;  $T$  is a variable relaxation delay. For  $t_1 \geq 2T_c$ , scheme A is substituted with B. The dashed pulses during delays  $T$  are optional. The durations and strengths of the  $z$ -gradients in units of (ms; G/cm) are: G1 = (1; 7.5), G2 = (0.5; 10), G3 = (1; -8), G4 = (0.5; 6), G5 = (0.5; 18), G6 = (0.5; 30), G7 = (0.3; 2.5), G8 = (0.3; 7), G9 = (0.125; -29.5). The phase cycle is:  $\phi_1 = x, y, -x, -y$ ;  $\phi_2 = x, 2(y), 2(-x), 2(-y)$ ;  $\phi_4 = x$ ;  $\phi_5 = -y, y$ ;  $\text{rec} = x, -x, -x, x$ . Quadrature detection in  $F_1$  is achieved with a gradient-enhanced sensitivity scheme<sup>49,50</sup> by recording a pair of data sets with  $(\phi_4, G_9)$  and  $(-\phi_4, -G_9)$  for each  $t_1$  point. For each successive  $t_1$  value,  $\phi_2$  is inverted.<sup>51</sup> (b,c) Comparison of spectra obtained using (b) the pulse scheme of Figure 2 (inset A,  $T = 0$ , Ile $\delta$ 1- $^{13}\text{CH}_2\text{D}$ -MSG), and (c) the pulse-scheme of this Figure ( $T = 0$ , Ile $\delta$ 1- $^{13}\text{CHD}_2$ -MSG), 600 MHz, 37 °C. The CHD<sub>2</sub> data is multiplied by a factor of 2.5 to achieve the same noise level in both data sets. Peaks marked with  $\oplus$  belong to the second conformation of Ile 309.

general, the sensitivities of the data sets associated with measurements involving the relaxation of  $D_+D_z + D_zD_+$  and  $3D_z^2 - 2$  are approximately a factor of 1.7 lower than for  $D_+$  and  $D_z$ , consistent with previous observations,<sup>15</sup> and fewer (32 versus 36) correlations could therefore be quantified in measuring the relaxation of these “rank-2” interactions.

One of the main advantages of  $^2\text{H}$  spin relaxation is that, because a large number of measurements can be performed at a given methyl site (up to 5), it is possible to verify the consistency of the data prior to an analysis in terms of motional parameters.<sup>15,16</sup> Jacobsen and co-workers have shown that so long as  $J(0) \geq J(\omega_D) \geq J(2\omega_D)$ , where  $J(\omega_D)$  is the spectral density function evaluated at the  $^2\text{H}$  Larmor frequency,  $\omega_D$  (see Materials and Methods section), the following inequalities must hold:<sup>26</sup>  $(5/3)R^Q(D_+D_z + D_zD_+) \geq R^Q(D_+) \geq (5/3)R^Q(3D_z^2 - 2) \geq R^Q(D_z)$ . Figure 5a,b shows that this is indeed the case for all Ile methyls in MSG. In applications involving high molecular weight proteins the “inequality test”,  $(5/3)R^Q(D_+D_z + D_zD_+) \geq R^Q(D_+)$ , is not rigorous. For example, using the simple expression for the spectral density function of eq 2, along with  $\tau_c = 56$  ns and average motional parameters for MSG ( $S_{\text{axis}}^2 = 0.6$ ;

$\tau_f = 20$  ps, 37 °C),  $R^Q(D_+)$  and  $R^Q(D_+D_z + D_zD_+)$  are calculated to differ by only 1.3%, with the difference growing to 3.5% for  $\tau_f = 100$  ps. Such small differences are within the errors of the measurement, so that unless there is a severe problem with the data the inequality  $(5/3)R^Q(D_+D_z + D_zD_+) \geq R^Q(D_+)$  will always be satisfied. A more telling test is if the data satisfy the consistency relation,<sup>26</sup>  $R^Q(D_+D_z + D_zD_+) = R^Q(D_+) - (2/3)R^Q(3D_z^2 - 2)$ . For large proteins  $R^Q(D_+) - (2/3)R^Q(3D_z^2 - 2) \approx R^Q(D_+)$ , and in the case of MSG we have directly compared relaxation rates for  $D_+$  and  $D_+D_z + D_zD_+$  and the corresponding squared order parameters,  $S_{\text{axis}}^2$ , that are derived from them. A plot of  $R^Q(D_+)$  versus  $R^Q(D_+D_z + D_zD_+)$  for 33 Ile $\delta$ 1 residues that could be quantified in MSG is shown in Figure 5c with an excellent correlation between measured rates.

The close correspondence between  $R^Q(D_+)$  and  $R^Q(D_+D_z + D_zD_+)$  (Figure 5c) indicates that on average the contributions to transverse relaxation from picosecond time scale dynamics (i.e.,  $\tau_f$ ) are small. To good approximation,  $R^Q(D_+)$  and  $R^Q(D_+D_z + D_zD_+)$  report directly on  $S_{\text{axis}}^2$ , while  $R^Q(3D_z^2 - 2)$  and  $R^Q(D_z)$  are sensitive primarily to  $\tau_f$ . Therefore,  $S_{\text{axis}}^2$  can be accurately estimated via

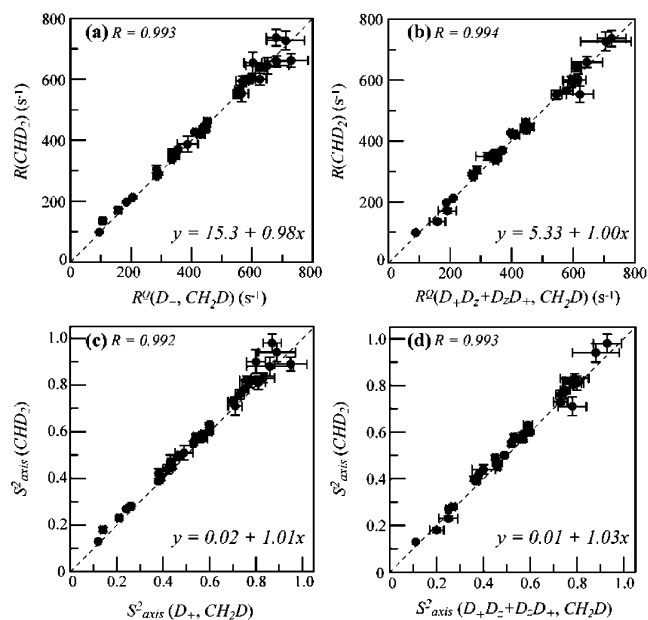
$$R^Q(D_+) \approx R^Q(D_+D_z + D_zD_+) \approx \left(\frac{1}{80}\right)\left(\frac{e^2qQ}{\hbar}\right)^2 S_{\text{axis}}^2 \tau_c \quad (7)$$

Figure 5d shows the excellent correlation obtained for the  $R^Q(D_+)$ - and  $R^Q(D_+D_z + D_zD_+)$ -derived  $S_{\text{axis}}^2$  values using eq 7 with  $\sum_i A_i \tau_i$  (see Materials and Methods section, eq 2) substituted for  $\tau_c$  to account for the anisotropy of rotational diffusion, although the assumption of isotropic tumbling makes only small changes to the resulting  $S_{\text{axis}}^2$  values. A very similar correlation is obtained by fitting rank 1 [ $R^Q(D_+)$ ,  $R^Q(D_z)$ ] and rank 2 [ $R^Q(D_+D_z + D_zD_+)$ ,  $R^Q(3D_z^2 - 2)$ ] experimental  $^2\text{H}$  rates separately to the complete expressions for relaxation (eqs 1a–e) using the spectral density function of eq 2 (inset to Figure 5d). The difference between  $S_{\text{axis}}^2$  values derived using the two approaches is 2.9% on average (1.2% upon elimination of four residues with  $S_{\text{axis}}^2 < 0.3$ ), which is slightly smaller than the average error in the derived  $S_{\text{axis}}^2$  values, 3.3%.

The correlations in Figure 5 establish that robust values of  $S_{\text{axis}}^2$  can be derived from either the measurement of  $R^Q(D_+)$  or  $R^Q(D_+D_z + D_zD_+)$ . Interestingly, values of  $\tau_f$  extracted from fits of [ $R^Q(D_+)$ ,  $R^Q(D_z)$ ], 18.6 ps on average, or [ $R^Q(D_+D_z + D_zD_+)$ ,  $R^Q(3D_z^2 - 2)$ ], 22.1 ps on average, show slight systematic deviations, although they are highly correlated (correlation coefficient of 0.95). The values of  $\tau_f$  obtained in this study are consistent with values for Ile residues measured in previous studies of methyl dynamics in our laboratory, but are smaller than average values for other residues such as Leu or Val by approximately a factor of 2.

All of the data presented to this point (and in what follows) were obtained using pulse schemes that did not include the  $^1\text{H}$ – $^{13}\text{C}$  180° pulses indicated by dashed lines in Figure 2. When these pulses were used essentially identical values were measured for  $R^Q(D_z)$  and  $R^Q(3D_z^2 - 2)$ , although a systematic decrease of  $5.1 \pm 3.3\%$  on average was observed for both  $R^Q(D_+)$  and  $R^Q(D_+D_z + D_zD_+)$ , corresponding to decreases in extracted  $S_{\text{axis}}^2$  values of close to 0.03. The origin of this difference is not clear; inclusion of the pulses did not influence transverse rates measured in protein L (25 °C,  $\tau_c = 5\text{ns}$ ) or transverse relaxation measurements using  $^{13}\text{CHD}_2$  probes (see later discussion). Detailed calculations suggest that they should in fact have little effect.

**Measuring  $S_{\text{axis}}^2$  Values Using  $^{13}\text{CHD}_2$  Reporters.** Previous  $^2\text{H}$  spin relaxation studies have focused on the  $^{13}\text{CH}_2\text{D}$  isotopomer as a probe of molecular dynamics,<sup>13,56–61</sup> as opposed to  $^{13}\text{CHD}_2$  methyls, and for applications involving small to intermediate size proteins (see later discussion) there is good reason.<sup>13</sup> In the case of  $^{13}\text{CH}_2\text{D}$  groups the presence of only a single deuteron makes it straightforward to construct experiments that measure directly the terms of interest, for example the decay of  $D_z$  or  $D_x$  in  $T_1$  and  $T_2$  experiments, respectively. In contrast, in the case of  $^{13}\text{CHD}_2$  moieties a more complex mixture of terms that depends on products of operators from deuteron spins 1 and 2 is obtained that may significantly complicate extraction of reliable dynamics parameters. One



**Figure 7.** Linear correlation plots of (a)  $R(^{13}\text{CHD}_2)$  (y-axis) vs  $R^Q(D_+, ^{13}\text{CH}_2\text{D})$  (x-axis) (b)  $R(^{13}\text{CHD}_2)$  (y) vs  $R^Q(D_+D_z + D_zD_+, ^{13}\text{CH}_2\text{D})$  (x), (c)  $R(^{13}\text{CHD}_2)$ -derived  $S_{\text{axis}}^2$  (y) vs  $R^Q(D_+, ^{13}\text{CH}_2\text{D})$ -derived  $S_{\text{axis}}^2$  (x), and (d)  $R(^{13}\text{CHD}_2)$ -derived  $S_{\text{axis}}^2$  (y) vs  $R^Q(D_+D_z + D_zD_+, ^{13}\text{CH}_2\text{D})$ -derived  $S_{\text{axis}}^2$  (x). Best-fit parameters from linear regression of the data (36 peaks in panels a,c and 32 peaks in panels b,d) are shown for each plot along with Pearson's correlation coefficient,  $R$ .

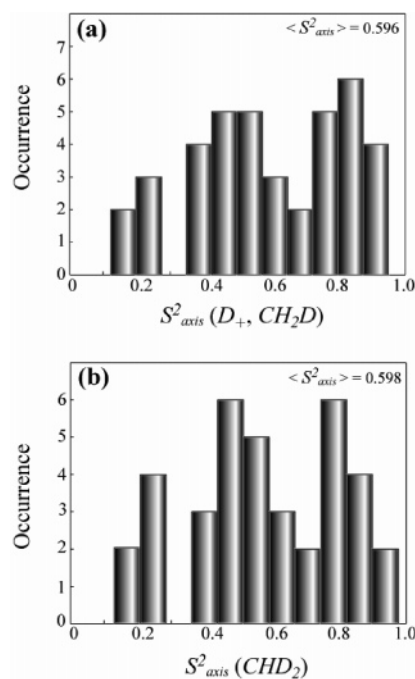


**Figure 8.** Histograms of  $S_{\text{axis}}^2$  values of Ile $\delta$ 1 methyls from MSG derived from (a)  $R^Q(D_+, ^{13}\text{CH}_2\text{D})$  rates and (b)  $R(^{13}\text{CHD}_2)$  rates. Average  $S_{\text{axis}}^2$  value for each distribution is indicated.

exception involves measurement of  $^2\text{H}$  transverse relaxation rates in applications involving high molecular weight proteins.

Figure 6a shows the pulse scheme that has been developed for the measurement of  $^2\text{H}$   $T_2$  values in large proteins. The basic scheme is similar to an enhanced sensitivity HSQC with additional elements inserted for the measurement of deuterium relaxation. Between points *a* and *b* of the sequence, evolution of  $^{13}\text{C}$  magnetization proceeds due to the  $^{13}\text{C}$ – $^2\text{H}$  scalar

(56) Kay, L. E.; Muhandiram, D. R.; Wolf, G.; Shoelson, S. E.; Forman-Kay, J. D. *Nat. Struct. Biol.* **1998**, *5*, 156–163.

(57) Ishima, R.; Louis, J. M.; Torchia, D. A. *J. Mol. Biol.* **2001**, *305*, 515–521.

(58) Ishima, R.; Petkova, A. P.; Louis, J. M.; Torchia, D. A. *J. Am. Chem. Soc.* **2001**, *123*, 6164–6171.

(59) Lee, A. L.; Wand, A. J. *Nature* **2001**, *411*, 501–504.

(60) Lee, A. L.; Kinnear, S. A.; Wand, A. J. *Nat. Struct. Biol.* **2000**, *7*, 72–77.

(61) Desjarlais, J. R.; Handel, T. M. *J. Mol. Biol.* **1999**, *290*, 305–318.

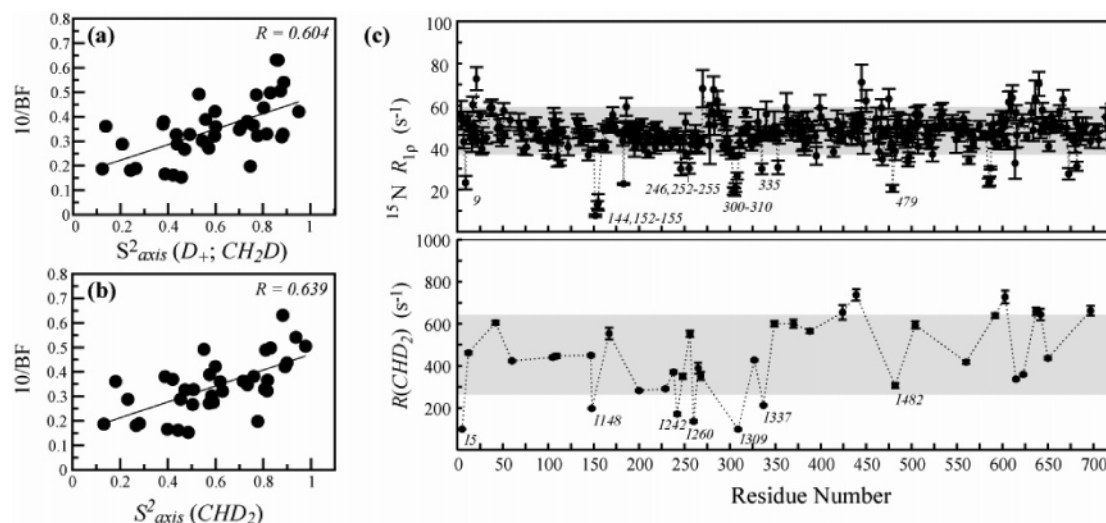


**Figure 9.** Linear correlation plots of (a)  $R(D_+, ^{13}\text{CH}_2\text{D})$ -derived  $S_{\text{axis}}^2$ , (b)  $R(^{13}\text{CHD}_2)$ -derived  $S_{\text{axis}}^2$  vs  $10/\text{BF}$ , where BF are temperature-factors of Ile $\delta^1$  atoms from the X-ray structure of MSG in complex with magnesium and glyoxylate<sup>18</sup> (PDB ID 1d8c). (c) Backbone amide  $^{15}\text{N}$   $R_{1\rho}$  rates (top) and Ile $\delta^1$   $R(^{13}\text{CHD}_2)$  rates (bottom) plotted vs residue number. Shaded areas indicate the regions within 1 standard deviation of the mean.

couplings involving the carbon and its attached pair of deuterons so that at point *c* the terms of interest are

$$-[C_z(D_{y,1} + D_{y,2})] \sin(4\pi J_{\text{CD}} T_C) - [C_z(D_{y,1}^2 D_{y,2} + D_{y,1} D_{y,2}^2)][0.5 \sin(8\pi J_{\text{CD}} T_C) - \sin(4\pi J_{\text{CD}} T_C)] \quad (8)$$

where the subscripts 1 and 2 above are used to distinguish the two deuterons. Following a relaxation delay  $T$ , carbon chemical shift is recorded and magnetization is refocused with respect to the coupled deuterons prior to the transfer to protons for detection.

It is noteworthy that the terms present during the relaxation delay,  $T$ , are not all of the form  $D_{y,i}$  that we might associate with measurement of  $T_2$  relaxation rates. Nevertheless, it can be shown that in the limit where  $J(0) \gg J(\omega_D)$ ,  $J(2\omega_D)$  each of  $D_{y,i}^2 D_{y,j}$ ,  $D_{y,i}$  relaxes monoexponentially with a rate that is identical to the rates of decay for  $D_+$  and  $D_+ D_z + D_z D_+$ . Computations establish that accurate measures of  $^2\text{H}$   $T_2$  relaxation rates are possible (less than 1% error) for  $\tau_c$  values in excess of  $\sim 25$  ns ( $S_{\text{axis}}^2 = 0.6$ ,  $\tau_f = 40$ ps) although even for smaller correlation times the errors are calculated to remain reasonably small ( $< 2.5\%$  for  $\tau_c = 10$  ns,  $S_{\text{axis}}^2 = 0.6$ ,  $\tau_f = 40$  ps). Not surprisingly, simulations also establish that the relaxation rates of  $C_z D_{y,i}^2 D_{y,j}$  or  $C_z D_{y,i}$  and  $D_{y,i}^2 D_{y,j}$ ,  $D_{y,i}$  are essentially identical (i.e., relaxation contributions from “ $C_z$ ” are negligibly small).

The signal-to-noise in data sets recorded with the scheme of Figure 6 can be maximized by ensuring that the transfer of magnetization from  $^{13}\text{C}$  to  $^2\text{H}$  and back is optimal. The net transfer function for the combined out and back process (neglecting  $^{13}\text{C}$  relaxation) is given by  $2 \sin^2(8\pi J_{\text{CD}} T_C) + 4 \sin^2(4\pi J_{\text{CD}} T_C)$  and has a maximum when  $T_C \approx 1/(12J_{\text{CD}})$ . Thus, taking into account only the transfer efficiencies during the pair of  $2T_C$  periods, one-half of the original magnetization at point *a* of the sequence can be refocused at the end. This is to be contrasted with two-thirds of the signal in the case of a single deuteron. However, unlike the  $^{13}\text{CH}_2\text{D}$  methyl-TROSY version where a factor of  $2\sqrt{2}$  in sensitivity is lost at the outset (see above), there is no such penalty for the present experiment,

leading to sensitivity gains. Figure 6b,c compares  $[^1\text{H}, ^{13}\text{C}]$  correlation maps recorded on samples of Ile $\delta^1$ - $[^{13}\text{CH}_2\text{D}]$  MSG (scheme of Figure 2, inset A,  $T = 0$ ) and of Ile $\delta^1$ - $[^{13}\text{CHD}_2]$  MSG (scheme of Figure 6,  $T = 0$ ). The spectra were acquired using acquisition parameters optimized separately for each experiment and are scaled in Figure 6 so that the noise floors in each are identical. The spectra obtained for the  $^{13}\text{CHD}_2$  sample are on average 30–40% more sensitive (normalizing for the slightly different measuring times; for several peaks, for example I603 and I697, much higher increases (3 to 4) in signal-to-noise ratios were obtained), although resolution is certainly inferior. The decrease in resolution is primarily the result of dipolar interactions involving intramethyl  $^{13}\text{C}$  and  $^1\text{H}$  spins that are not suppressed during the  $t_1$  evolution period in the scheme of Figure 6 but are in the experiments of Figure 2 (eq 5b).

As described earlier, excellent agreement between transverse relaxation rates measured using the schemes of Figure 2 (A, C),  $R^Q(D_+)$  and  $R^Q(D_+ D_z + D_z D_+)$ , and Figure 6,  $R(^{13}\text{CHD}_2)$ , is expected so long as  $J(0) \gg J(\omega_D)$ ,  $J(2\omega_D)$ . Figure 7 shows that this is indeed the case. Similarly,  $R(^{13}\text{CHD}_2)$ -derived  $S_{\text{axis}}^2$  values are in good agreement with those derived from  $R^Q(D_+)$  and  $R^Q(D_+ D_z + D_z D_+)$  in  $^{13}\text{CH}_2\text{D}$ -labeled samples (Figure 7c,d). The small systematic differences in rates and order parameters between values obtained from  $^{13}\text{CH}_2\text{D}$  and  $^{13}\text{CHD}_2$  probes likely reflect minor variations in protein concentrations between the two samples and small errors in estimated correlation times.

**Distribution of  $^2\text{H}$ -Derived  $S_{\text{axis}}^2$  Values in Isoleucine Side Chains of MSG.** Histograms of  $^{13}\text{CH}_2\text{D}$ - and  $^{13}\text{CHD}_2$ -derived  $S_{\text{axis}}^2$  values of Ile residues in MSG are shown in Figure 8a,b. A clear three-mode distribution is observed,<sup>59</sup> which is more obvious than that obtained from a combined data set based on experimental results compiled for 18 proteins.<sup>62</sup> Of course, such a distribution can be directly observed from the transverse relaxation data (Figures 5c and 7a,b). Recently Best et al. have used molecular dynamics simulations to provide insight into the dynamics that underly the pattern of observed  $S_{\text{axis}}^2$  val-

(62) Mittermaier, A.; Kay, L. E.; Forman-Kay, J. D. *J. Biomol. NMR* **1999**, *13*, 181–185.

ues.<sup>19</sup> They note that the three modes derive from the following: (i)  $\chi_1, \chi_2$  dynamics limited to excursions within their respective wells (high  $S_{\text{axis}}^2$ ), (ii) only  $\chi_2$  undergoes jumps (medium  $S_{\text{axis}}^2$ ), and (iii) motion about  $\chi_1$  that involves jumping between wells (low  $S_{\text{axis}}^2$ ). The larger-than-average number of Ile  $\delta 1$  methyls in MSG with  $S_{\text{axis}}^2 > 0.70$  than what has been observed in other proteins may reflect the large hydrophobic core of the enzyme with side chains constrained by tight packing.<sup>18,23</sup> A weak, but statistically significant, correlation between Ile  $S_{\text{axis}}^2$  values and the degree of packing or occluded surface area of Ile side chains (estimated with the program OS<sup>63</sup>) has been observed in MSG. Interestingly, a reasonable correlation between  $S_{\text{axis}}^2$  values and the inverse of crystallographic B-factors for Ile C $\delta 1$  atoms is noted (Figure 9a,b). Not surprisingly, side chains with the lowest  $S_{\text{axis}}^2$  values (no preferred  $\chi_1, \chi_2$  rotamer occupancies or at the very least dynamics involving  $\chi_1$  torsion angle jumps) are often those belonging to partially disordered backbone segments of the protein sequence. Figure 9c illustrates the correspondence between the residues with the lowest backbone  $^{15}\text{N}$   $R_{1\rho}$  rates and the lowest  $R(^{13}\text{C}\text{H}\text{D}_2)$  rates in MSG.

In summary, we have presented new solution NMR pulse schemes for  $^2\text{H}$  relaxation measurements in  $^{13}\text{CH}_2\text{D}$  and  $^{13}\text{CHD}_2$  methyl groups of high molecular weight proteins. The approach

exploits recently developed labeling methods that provide very high levels of incorporation of the methyl isotopomer of interest.<sup>40</sup> Order parameters, obtained for Ile  $\delta 1$  methyl groups in MSG from a variety of different experiments using different methyl isotopomer probes, are shown to be in good agreement. A distribution of side-chain dynamics is obtained that is consistent both with previous experimental studies<sup>62</sup> and with molecular dynamics simulations.<sup>19</sup> The methods developed significantly extend the range of systems for which side-chain dynamics can be quantified and represent an important contribution to the growing list of NMR approaches for the study of complex macromolecules.

**Acknowledgment.** This work was supported by a grant from the Canadian Institutes of Health Research (CIHR) to L.E.K. V.T. and J.O. acknowledge the support of the Human Frontiers Science Program (HFSP) and the Natural Sciences and Engineering Research Council of Canada, respectively. We thank Drs. O. Millet (University of Barcelona, Spain) and D. M. Korzhnev (University of Toronto) for helpful discussions. We are particularly grateful to Prof. N. R. Skrynnikov (Purdue University, IN) who realized that a planar-TOCSY scheme could be used to improve the sensitivity of correlation maps involving  $^{13}\text{CH}_2\text{D}$  methyls. L.E.K. holds a Canada Research Chair in Biochemistry.

JA0508830

(63) Fleming, P. J.; Richards, F. M. *J. Mol. Biol.* **2000**, *299*, 487–498.